Visualization of slip mechanisms at low sliding velocities

by

Dwarkanath Pramanik

1st March 2011

Contents

Chapter 1

Introduction and motivation

The study of friction in modern physics has gone on for nearly half a millennium, starting with Leonardo Da Vinci's work during the 1500s. His work was aided by the efforts of Amontons and Coulomb, and resulted in three main laws of friction. These laws are still taught as part of the high school curriculum in physics. Much progress has been made since the time of Da Vinci, but the general consensus in the field of tribology is that this phenomenon warrants continued investigation. Because, although a reasonable understanding has been developed, there is indeed a lot more to be done to fully decipher and entirely understand the fundamental aspects of friction. For instance, relatively little is known about the exact mechanics and behavior at low sliding velocities between two surfaces in contact. At the moment there still does not exist a general method for calculating the coefficient of friction.

With the introduction of their Micro Contact Interface model (MCI) during the 1940's, Bowden and Tabor provided a new framework for explaining the presence of friction and its independence of the observed area of contact[19]. In their paper 'Theoretical Study of Friction: A Case of One-Dimensional Clean Surfaces' Matsukawa et al. suggested a technique to estimate kinetic and static friction forces for a stationary states[13]. This was achieved by summing all of the forces for atomic interactions between two bodies made up of point particles. They also noted a connection between kinetic friction forces and their dependency on velocity. This dependency vanishes as the strength of interatomic forces grows between the two bodies, meaning that maximum static friction force also increases.

This study of friction is part of a larger field known as tribology which is a sub-branch of mechanical engineering and includes the study of adhesion, lubrication and wear. Research has shown that behavior of friction related effects are more complicated than they may initially appear. The practical use of this knowledge is relevant for a deeper understanding and application in areas as diverse as earthquake predictions (seismology), several industrial applications and biological systems, i.e. from extremely large scale systems to microscopic systems [19]. There is a striking similarity between the type of lubrication and friction forces observed in internal organs of animals and various biological microstructures that are also found inside manmade machines [15]. Unfortunately, it is also often the case that friction and wear can incur a financial loss for example in the form of material and energy. This is not only the case with machinery and other manufactured things, but also in the human body. Artificial teeth, skeletal joints and heart valves enhance the conditions of human life when biological parts become damaged and need to be replaced [11].

Lately significant progress has been made for research linked with theoretical modelling attempting to fuse seemingly different phenomena and clarify less obvious and and often counter-intuitive features (due to the nonlinear nature of the problem) of moving matter [15]. Studies show that formation of strong junctions takes place between sliding surfaces at the points of contact. For sliding friction these contacts are repeatedly broken and reformed. Despite the fact that workings of this mechanism lacks understanding, it is certain that plastic deformation and fracture is involved. Deducing a clearer perception of these of phenomena relating to friction is important for gaining a better understanding of sliding friction. Recently, two-dimensional experimental studies have been able to measure the change in the effective contact area during the onset of frictional slip [20, 18]. This introduces a good opportunity for calibrating and testing numerical models for the detailed dynamics of the slip surface. Although the measurements conducted are two-dimensional, the real system is three-dimensional. Therefore it is essential to study the dynamics of complete three-dimensional systems in order to understand their dynamic instabilities and how these are reflected in a two-dimensional observation method.

My main goal in this thesis is to look at what happens between two slid-

ing surfaces at the macroscopic level for sliding at a low and steady velocity. This will be followed by a detailed description of my findings with emphasis on the graphical presentation that I find most appropriate to describe the results with. To accomplish this I will develop a discrete element method (DEM) to serve as a tool for the investigation at hand. More specifically, this will be implemented as a slider spring model (see Chapter 4 for a detailed description), which has become a common method for these type of studies. More complicated models are available and in use, but for my task the chosen model will suffice because the relevant dynamics that take place can be created with it.

In the past, it seems that the majority of tribological studies has been done with actual physical models. However, in recent years the massive growth in computing power has made the field of computational physics an essential approach to almost every branch of science, be it economical analysis or quantum physics. Numerical simulations has therefore become an equally valid alternative to the type of experiments mentioned above. For example in molecular dynamics (MD) simulations. To name a few of the reasons to use numerical simulations, cost efficiency, ease of data collection, highly flexable system properties, etc. Another major advantage with numerical experiments is repeatability, so that similar experiments can be carried out several times (and in parallel) without too much extra effort.

The following chapter gives an overview of the historical development of friction theory starting with Da Vinci and Amonton's laws up to more recent discoveries, such as state dependent friction laws. I will also describe and explain some of the key concepts that relate to my work in addition to some general theory such as stick slip, geometric aging etc.

Chapter 4 gives a detailed description of the model I will be working with in this project. Chapter 5 deals with the numerical setup and details of the algorithm. This chapter gives a fairly detailed breakdown of the most important parts of the program. Although the results are paramount, it is in my opinion important to show in the manner they were achieved and considering the time that was spent on this phase it is most appropriate. Chapter 6 describes the calibration of the system. Chapter 7 provides a short look testing of the system. In Chapters 8 and 9 I present and discuss my results. Lastly, in Chapter 10 I reflect on the project as a whole and give some concluding

remarks.

Finally, I would like to thank my supervisor Professor Anders Malthe-Sørenssen for his guidance and support during this undertaking. Other people who have been most supportive and helpful during this project are Eirik Hanssen, Ishita Barua and Professor Morten Hjort-Jenssen. And special thanks must given to my fellow students Andreas Birkeli, Lars Eivind Lervåg, Yang Min Wang and Sigurd Wenner for invaluable help and input.

Chapter 2

Historical and Theoretical Overview

2.1 Early Development

The practical use of friction has been known since the stone age when humans used frictional heat to light fires. Leonardo da Vinci (1452-1519) did some of the first known systematic studies of friction in modern times. In his experiments he measured the friction force F needed to slide a mass M across a surface. The material combinations he used were mainly wood on wood and wood on iron. His findings suggested that the dependence of friction between any two materials is directly proportional to the applied normal load N and independent of the geometrical area of contact A_r (i.e the force was independent of the positioning on surface). As of yet, no theory has provided a satisfying explanation for this law, all attempts have been dependent on the system or model being used. These observations were rediscovered by Guillaume Amontons in 1699 and expanded upon [9]. One of the materials used by Amontons for his experiments was wood (like da Vinci used). At the time wood was assumed to be a single chemical entity. But as we know now, the structure and composition of wood consists of a mix of cellulose, hemicellulose and various organic and inorganic substances among other things [6].

Consequently there are two laws known as da Vinci-Amontons laws. Later, Charles-Augustin de Coulomb (1736-1806) discovered that the friction force is also independent of the sliding velocity. These three observations can be

summarized in the following way [14] [13]:

1. **Independence of the area of contact**
   Friction is independent of the apparent area of contact.
2. **Amonton's Law**
   Friction is proportional to the applied load. The ratio $\mu = F_L/F_N$ is called the coefficient of friction. It is (usually) larger larger for static friction than for kinetic friction. Normally its value, which is material dependent, lies in the range between 0.2 and 0.8.
3. **Coulomb's Law**
   The kinetic friction is independent of the relative velocity of the contact surfaces, and is less than the maximum static friction force.

Some of these laws appear to be counterintuitive and the behavior of certain friction related phenomena might be deceptive at first. These three fundamental laws which are derived from macroscopic experiments, have yet to be fully understood in terms of more fundamental microscopic processes. Presently, several cases are known when these laws of friction are no longer valid.

2.2 Departures from Amonton's law

Some of the instances where Amonton's law in no longer valid can be attributed to [12]:

1. The dependence of the friction coefficient μ on the normal pressure N, i.e. , $\mu = f(N)$
2. The dependence of the static friction force F_s on the duration of stationary contact t_0, i.e $F_s = f(t_0)$
3. The dependence of the friction force F on the velocity v, i.e $F = f(v)$

4. The dependence of the friction force F on the sliding time t, i.e $F = f(t)$

With the exception of number 1, none of these exceptions occurs when the sliding time is sufficiently short, i.e. $t \to 0$.
Various endeavours were made to account for Amontons law, by Amontons, Coulomb and Euler among others. These attempts were done by investigating the mechanics of two surfaces sliding across each other. For sliding motion to occur the asperities of one surface would have to "climb" across the asperities of the other surface. The lateral friction force required to elevate such an asperity is given by $F_i/L_i = \tan\theta_i$ for the i-th asperity.Where θ is the maximum slope of the asperity junction and L is the local normal load. It is not unreasonable to make the approximation that the average value of θ is constant, i.e $\langle\tan\theta\rangle = constant$. From this assumption we can calculate the total frictional force F where N is the total normal load

$$F = \sum F_i = \sum N_i \tan\theta = \langle\tan\theta\rangle N = \mu N \ . \tag{2.1}$$

For the third equality they assumed "that on average the local values of $\tan\theta_i$ and N_i are uncorrelated". In the equation above one can see that no mention of the contact area A or sliding velocity v is made. This implies as stated before that the macroscopic friction coefficient μ is independent of these parameters. Neither does this line of argument account for adhesion effects. However, not long after a number of arguments were made questioning the experimental and theoretical validity of this view presented to disprove this entirely mechanistic and geometrical approach to friction. Among others, Sir John Leslie (1766-1832) argued that the energy used to push (or drag) an asperity over another would be regained once it fell down on the other side. So, there would be no change in the total energy. Once the two surfaces were set in motion, no driving force would be needed as the friction force would be nonexistent. Clearly, there had to be some other mechanism responsible for the dissipation of energy [9].

As mentioned, Coulomb found that dry friction is independent of velocity. Dry, Coulomb or unlubricated friction is the instance when there is no lubrication between the surfaces in contact. The opposite case known as wet, viscous or lubricated friction is when there is a lubricant separating the moving surfaces. Coulomb also suggested that friction is a result of roughness on

the micrometer scale. This was later contested by Desaguliers and he presented molecular adhesion as an alternative explanation. Molecular adhesion is proportional to the contact area while friction is known to be independent of the contact area. In the 1950s Frank Philip Bowden and David Tabor solved this discrepancy. The results from their tribological experiments led them to introduce the concept the real area of contact. This concept is still a valid and useful tool for the majority of ongoing tribological research.

Bowden and Tabors model says that friction is proportional to the real area of contact. This area is not the same as the apparent contact area. When the normal force increases, the number of asperities also increase. This model is also able to account for the da Vinci-Amontons law, yet it is unable to answer fundamental questions. Desaguliers was not far off in assuming that adhesion is related to friction rather than the roughness of the surface. Because adhesion effect also are proportional to the contact area, this model is known as the Bowden-Tabor adhesion model.

In the past decade or so new tools and apparatus such as the friction force microscope has been developed to address these and other questions. New phenomena like stick-slip on the atomic scale, stick-slip in relation to phase transitions and asperity creep were discovered. Also computer simulations and molecular dynamics in particular proved very useful in the visualization and unlocking of these intricate processes.

2.3 Bowden and Tabors discoveries

With the introduction of their Micro Contact Interface model (MCI) during the 1940's Bowden and Tabor provided a framework for explaining why there is a coefficient of friction and its independence of the observed area of contact [19]. They proposed that because of surface roughness the geometric or real area of contact can be thought of as a large number of micro-contacts. This net area formed by such micro-contacts simply constitutes a small fraction of the assumed contact area, and is the mechanism behind the frictional force. The sum of the total area that is created is independent of surface roughness and geometric properties of the material. Only the applied normal load and mechanical properties of the material are relevant when determining the real area of contact.

For two bodies that are gradually brought together, the asperities the asperities with the greatest height are the first to touch. Thus, the load is supported at these contact points, that cling together as a result of interatomic forces. If the pressure at such a point exceed the "microscopic yield stress" of the material, the contact points will from junctions by welding together. Initially the deformation is elastic, resulting in an increase of the net contact area. But for pressures close to the yield stress the deformation becomes plastic also causing a growth of the net contact area and material flow. By multiplying the shear strength of each contact with the total area it is possible to estimate the maximum static frictional force. Because of this the maximum static frictional force is proportional to the normal load. Presently it is known that for metals that the sliding friction is primarily a result of strong adhesion in the real area of contact. This knowledge has also been drawn upon to explain the frictional properties of a variety of non-metallic systems [6].

However, this view is not applicable to a plain surface without any randomness, including at the atomic scale. Because the interatomic forces working between two bodies acts on all atoms at a surface, the frictional force will persist despite a disappearing normal load. Gravitational forces can be disregarded due their negligible contribution relative to the other forces involved. For such a surface all points will lose contact simultaneously, causing the first and second laws of friction to be violated [13].

2.3.1 Measuring the real area of contact

Measuring the real area of contact A_r can be a intimidating task. Since the majority of surfaces, be it natural or artificial normally have a roughness on a large number of length scales. Thus, describing such an intricate geometry in an easy way is also very difficult. Commonly used quantities such as the root-mean-squared (rms) roughness, slope and curvature, are determined by the length scale over which they are taken. Such values frequently tend to diverge for large and small scales. Although a partial remedy is to make estimates for selected topographies they are usually hard to generalize. Alternatively one can use less complicated models with roughness on a wide range of length scales known as self-affine fractals [10].

2.4 Unanswered questions and future development

Urbakh et al. define some longterm goals for tribology such as finding a unified approach to energy-dissipating systems. A necessary feature of such a system should be that it can account for general tribological phenomena, but also other sciences such as biology and geology. Such models need to elucidate general results and discoveries that can be complex in their nature. This will make us able to clarify how energy dissipation works and predict future results.

They also suggest that some of the following important questions should be answered [15]:

1. Why is static friction so universally observed between solid objects?
2. How are friction and wear related? And why does surface damage often occur at the start of motion?
3. How are the static and kinetic friction forces, and the characteristic transition velocities between smooth and stick-slip sliding, determined by the molecule-molecule and molecule-surface interactions and, in macroscopic systems, asperity-asperity or grain-grain interactions?
4. Are the stick and slip regimes indicative of different phase states (liquid, solid, glassy) of the confined films or interfaces?
5. What hidden information is contained in chaotic as opposed to periodic motion. This is particularly important for predicting earthquakes.
6. And finally, how can we control friction in practice, most often to reduce it or eliminate stick-slip at all pressures and velocities?

.

2.5 Detachment fronts and slip dynamics

In 2006 Rubinstein et al. investigated the mechanics of what takes place between a sliding-block and a base made from the same material.

Specifically, during the onset of frictional slip [19]. This is useful as there are some differences in the type of processes during this phase compared to what happens during sliding at a steady velocity.

The dimensions of the polymethylmethacrylate (PMMA) slider was $100 \times 6 \times 75$ mm, and the size of the base was $300 \times 27 \times 30$ mm. Both of the surfaces in contact had a roughness of up to 2 μm (rms) which was created mechanically. A variable normal load F_N between 1 to $10MPa$ was uniformly distributed on the top of slider. Additionally, a shear force F_S was also applied, varying from 0 to $3MPa$.

By illuminating the interface with a laser and measuring the intensities of the reflected and transmitted light they were able to confirm Bowden and Tabors assumptions from the MCI theory. Because the exponential decay length of the reflected light is much smaller than the interface roughness, the intensity of the transmitted light thus provides a measure of the net contact area. The relationship between these two quantities were found to be linear, as can be seen in Figure 2.1

Their measurements revealed that right before the interface detachment process one can observe three different types of wave fronts. These three wavefronts can primarily be distinguished by their propagation velocity and the amount of reduction in contact area resulting from their passage along the interface.

They spread out along the interface from the trailing edge to the leading edge and can be of the following type:

1. The fastest one of the observed, so called sub-Rayleigh fronts, starts moving at a velocity less than and accelerates up to the speed of sound in the material. However, the net reduction of the contact area behind the front is minimal (approximately 10 %). The area of contact ahead of the front does not change. The sudden suspension of this type of front is followed by the simultaneous emission of two other fronts.

2. The second fastest intersonic front moves at speeds significantly larger

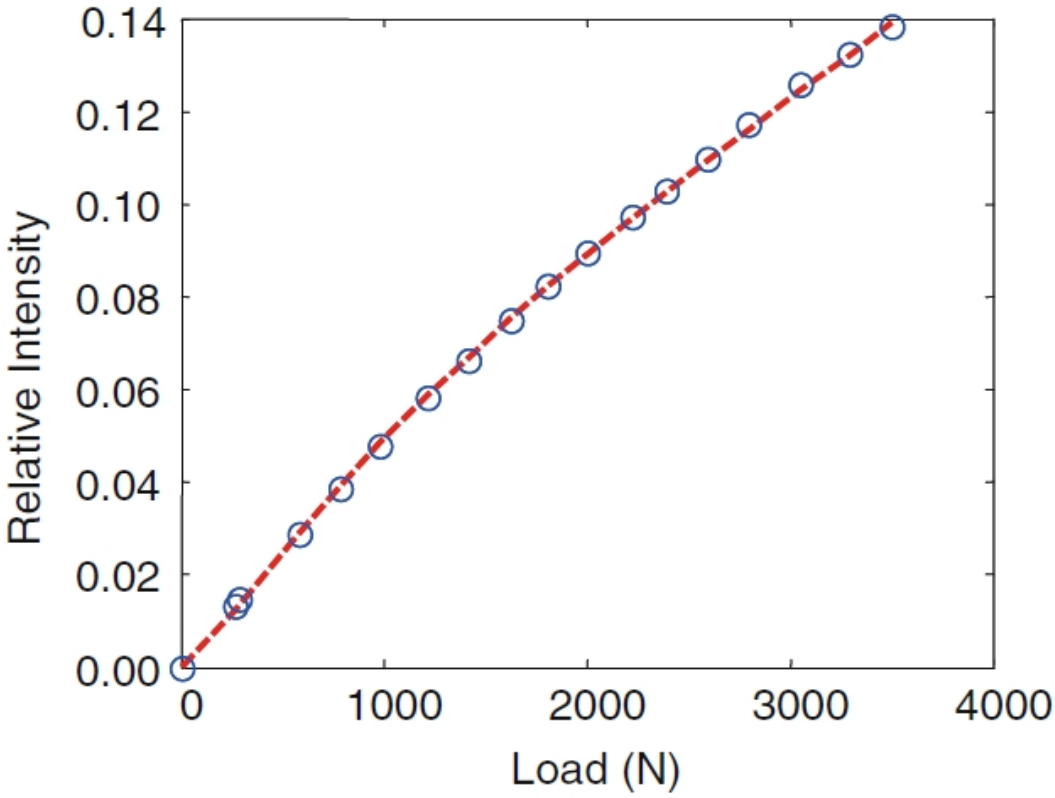

Figure 2.1: Transmitted intensity as a function of normal load F_N [19]

than the shear wave velocity. These fronts only result in a reduction of 1-2 % of thhere e contact area, despite propagating along the complete length of the interface. Because of this negligble amount of reduction this type of front is difficult to detect.

3. Slow-detachment fronts propagating at speeds 1-2 orders of magnitude slower than the Sub-Rayleigh fronts produce approximately a 20 % decrease of the contact area. The passing of such a front also causes a significant amout of slip preciding the overall motion of the slider.

Extremely short time scales dominate and thus describe these kind of detachment processes.

In 2009 Zapperi et al. studied slip mechanics by the means of apparatus called a Quartz Crystal Microbalance (QCM) [4]. Lateral forces produced by the oscillations in the crystal along with thermal activation produced slip for a monolayer of Xenon sliding across a copper surface covering the crystal. Essentially, their results showed that a slip in the monolayer film starts out as a small local event caused by nucleation that gradually spreads out, finally creating a global slip.

Chapter 3

Rate and state variable friction laws

Although the previous seen approach to friction with constant values for μ_s and μ_k and is very useful, we saw in the previous chapter that there also is a number of cases where this view becomes insufficient. It is fair to say that these coefficients gives a somewhat crude description of frictional behavior. During the 1970s a very important and novel formulation of friction started forming. Largely due to Dietrich's research relating to rock friction and the inability of the current laws to explain his data, prompted the need for a new framework to account for his findings. Through the consolidation of the efforts of Rice and Ruina, and the work done by Dietrich, this new approach took form and culminated into a set of empirical constitutive formulations known as rate- and state-dependent laws.

In experiments pertaining to dynamic friction it was found that a controlled increase in slip velocity leads to an instant change in the frictional resistance. This change is proceeded by displacement dependent reduction in the frictional resistance, that finally settles into a new steady-state sliding friction. Also, the opposite can be observed for a controlled reduction of the slip speed. This type of reaction to variations in slip rate takes place for a large range of temperatures, pressures and sliding velocities [8]. Application of these laws has proven that regardless of the limited number parameters and plainness, they give a sufficiently accurate account for many central and complex features regarding low-velocity frictional dynamics, for a diverse selection of materials, such as granite or paper. This suggest the potential for

a unified and perhaps material-independent representation of mechanics at the microscopic level [1].

3.1 Theory

Two surfaces that are in contact can described by their relative velocity V and a state variable θ that evolves when the two surfaces slide past each other [21]. Two effects can be observed during laboratory friction experiments if the sliding velocity is altered for the dynamic coefficient of friction μ_k. Initially one can detect a so-called 'direct' effect or short-term rate dependence. Thus, if one increases the sliding velocity V, it is accompanied by a corresponding increase for the dynamic coefficient of friction. Similarly, if the sliding velocity is lowered, the dynamic coefficient of friction will decrease accordingly. This is what is known as rate-dependent friction or long-term rate dependence. Subsequent to the instant rate or 'direct' effect, the dynamic friction coefficient will evolve over time. It appears that a surface remembers its past state, but with time evolves toward another state. This is known as state-dependent friction. Generally, the short-term rate dependence is positive, whereas the long-term rate dependence is found to be negative [7, 5].

In the original law presented by Dietrich, contact time was considered a critical factor [2]. Therefore the time dependence of static friction was linked to the velocity dependence of sliding friction by a effective contact time. The contat time was found by taking the ratio of a critical slip distance D_c and the slip velocity V. D_c represents the slip required to update surface contacts. Thus the ratio of D_c over V denotes an average contact lifetime θ. This yields a relation between time and velocity dependence of friction, that can be expressed by:

$$\mu = \mu_0 + a \ln(\frac{V}{V_0}) + b \ln(\frac{V_0 \theta}{D_c}) \; . \tag{3.1}$$

Variations in sliding resistance mirrors changes in the contact area. The event of stick-slip instability represents an overall decrease of the contact area. It also results in a reduction of contact population age, because of the increase in the sliding velocity previous contacts get substituted for new ones. It has been found that a wide range of materials with different characteristics show qualitatively similar effects for their sliding history and frictional properties.

However, the reason for this has yet to be found [8].

3.1.1 Possible physical interpretations of the parameters

- μ_0 is the initial coefficient of friction and generally lies between 0.5 to 0.8 for most materials, relating to the steady-state slip at V_0.
- V_0 is the initial sliding velocity and V is the new sliding velocity.
- θ is the state variable containing information about average age of the population of asperity contacts. The unit for θ is time. In other words a characteristic contact lifetime which is the average elapsed time since the contacts existing at a given time were initially formed.
- The dimensionless constants a and b are empirically determined with values normally found in the range between 0.005 to 0.015 for rocks. a is related to the change in rate and b is related to the change in state.
- D_c is understood as the characteristic sliding distance needed to renew a contact population descriptive of an earlier set of sliding states, for a contact population conceived during a new sliding state. In support of this interpretation (assuming that contacts are circular) it was found that the average contact diameter deduced from the average area of a contact will always be roughly the same as D_c. Analysis of video images from simulations by Dieterich and Kilgore provide additional support for this view. An alternative formulation is that D_c is the distance necessary to reach a statistical steady state for the contact population and thereby stabilize friction following a variation in sliding conditions.

  It has been shown experimentally that D_c is nearly independent of slip speed and normal stress, but does depend on surface conditions. D_c becomes greater with growing surface-roughness and the size of particles between two surfaces in contact.

Eq 3.1 is not defined for $V = 0$. Regretably this is inconvenient for numerical calculations but agrees the view where friction is the normalized shear strength of a specified surface. In order to determine this value, both kinetic and static friction, the surface needs to experience slip. The ratios found by scaling the terms in Eq 3.1 by constants a and b, symbolize a relative

measure between the velocity and a reference velocity V_o, the sum of which represent the measured time and velocity dependence of friction [2].

For the model presented in Eq 3.1 truly stationary contact for static friction and strength recovery is not unaccounted for. Instead, time dependence for static friction and the velocity dependence for sliding friction is connected through an effective velocity extracted from a relation between D_c and the time of quasistationary contact.

Ruina put forth results to show that friction may display memory effects in some cases. Such an effect manifests as a critical slip distance needed to create a change from one value to another. So, from Ruina's point of view, slipping within the hold period is cause behind time dependence for static friction [2].

Two common ways are used to describe the time-dependent evolution of θ at constant normal stress. Also, a third law, not discussed here, exhibits symmetry along with aging related to changes in velocity was proposed by Perrin et al. in 1995. Dieterich expressed it in the follwing manner

$$\frac{d\theta}{dt} = 1 - \frac{v}{D_c}\theta \; . \tag{3.2}$$

Ruina presented an alternative law where velocity and slip as opposed to time were determining factors.

$$\frac{d\theta}{dt} = -\frac{v}{D_c}\theta \ln(v\theta/D_c) \; . \tag{3.3}$$

The two equations above show different behaviour for the static case where $v = 0$. While Eq. 3.2, predicts aging, implying that when $v = 0$, θ will increase linearly with time, μ will increase logarithmically. Ruinas description, Eq. 3.3, says that when the object is not moving, θ does not evolve [21]. The former formulation is frequently called the 'slowness law' or the Dieterich-Ruina law of evolution for the state variable. So Dieterich's model describes friction principally through time dependence and static friction. Ruina's model presents an opposing view, i.e for all variations in friction slipping must occur. This also includes strengthening during quasistationary contact. Both laws produce overlapping and coherent results even though there is a fundamental difference between the two views. In particular, how

friction evolves regarding the micromechanical analysis of the fundamental processes taking place[2].

3.1.2 Fading memory and steady state

Because θ progresses towards a steady state over D_c, a change in sliding conditions will cause the memory of a previous state to fade along this distance. Experiments by Dieterich and Ruina indicate that after sufficient sliding on virgin samples the memory appears to be only short term. If a surface has a slip history $\delta(t)$ with a observed response $\tau_1(t)$. After some random intervening sliding, the slip history $\delta(t)$ is repeated, then the response $\tau_2(t)$ will approach $\tau_1(t)$ after enough time or displacement has elapsed. That is, reproducible results can be achieved for a single surface just by repeating displacement history. The state variables θ_i represent the surface memory of previous sliding where $\vec{\theta} = \theta_1, \theta_2, ...$ Hopefully the number of state variables θ_i needed is small, where θ_i represents some type of average for presumably complicated surface state.

Fading memory indicates the presence of a steady state for a constant sliding velocity. The reason that repeatable results are found is because the same slip history is being applied repeatedly for steady sliding. Given enough time θ will evolve into a steady-state value θ_{ss} This value can be obtained by considering Eq 3.2 after sufficiently long periods of time. We see that the left hand side $\frac{d\theta}{dt}$ tends to zero and yields:

$$\theta_{ss} = \frac{D_c}{V} \ . \tag{3.4}$$

An possible interpretation of such a steady state is that for any value of V there exists respective state values $\theta_i^{ss}(V)$ and shear stress $\tau^{ss}(V)$ that θ_i and τ approach after enough time or displacement at a steady slip rate. Replacing the $\theta_{ss} = \frac{D_c}{V}$ into Eq 3.1, and combining constants the value of steady-state friction can be written as

$$\mu_{ss} = const + (a - b) \ln V \ . \tag{3.5}$$

The values of the parameters a and b are critical for describing the stability of a fault plane (and hence earthquake nucleation). If $(a - b) < 0$, then the final friction coefficient(as the sliding velocity is increased) will be less than

the initial friction coefficient. This fullfills a general requirement for stick-slip, hence is possible to develop an instability. This behavior is referred to as velocity weakening. Experiments with dynamic friction for rock and gouge indicates that sliding friction decreases with velocity. Results showed that rock surfaces displayed velocity-weakening friction over a vast range of velocities. For the instance where $(a - b) > 0$, an instability cannot develop, hence stable sliding will occur. This behavior is known as velocity strengthening. For some experiments conducted at faster velocities, friction of rock transitions to velocity strengthening, possibly from heating. But this has yet to be fully comprehended. Many of the numerical results found suggest that friction develops over a finite slip distance.

Studies of these laws have clarified and determined several important aspects, such as frictional state evolution, the effects of shear strain and displacement on various scaling parameters and frictional behavior. Also, inconsistencies for results found under various testing conditions has become much more clearly comprehended. Despite the extended application of the above laws, there are issues with scaling among other things. But the important thing is that they provide a connection between static and dynamic friction. These laws stem from investigations into rock friction and frictional instability as cause of stick-slip failure and the seismic cycle [21, 7, 2, 5].

The rate- and state-dependent friction laws describe the variations in dynamic friction coefficient for variations in slip velocity. It has been shown experimentally that the static friction coefficient also is time dependent. It is not possible to describe this behavior given a framework where the sliding velocity v is equal to zero.

Chapter 4

Model

4.1 The physical system

As mentioned in the introduction, the setup used in this project consists of a solid rectangular block of mass M being pushed in the positive x-direction along a rough surface by a piston. Between the piston and the slider there is a spring which transfers the forces. When the spring is compressed more than its given equilibrium length it will exert a force on the slider. Initially, the slider does not move. So the spring can be thought of as either attached to the block or the piston, but not both so that when the separation is greater than the equilibrium length there are no forces transmitted between them. The piston is implemented as a wall moving at a constant driving velocity v_w. Its mass can be thought to be of such a great value compared to the sliders mass that no significant force from the slider acts on it. Additionally, a normal load N can be added on the block.

4.2 The slider

I have decided to discretize a slider of total mass M into a cubic lattice consisting of $N_x \times N_y \times N_z$ spheres. L_x, L_y and L_z are the lengths of the slider along the x, y and z directions, respectively. Where $L_x = L_y = 2 \times L_z$. The x-axis is the horizontal length, the y-axis is the depth, and the z-axis is the vertical length. From this definition we get a cubic lattice with volume $L_x \times L_y \times L_z$. Each sphere has a diameter defined by $L_x/N_x = l_0$, where l_0 is the lattice constant. The density of the block's material is given by ρ, so

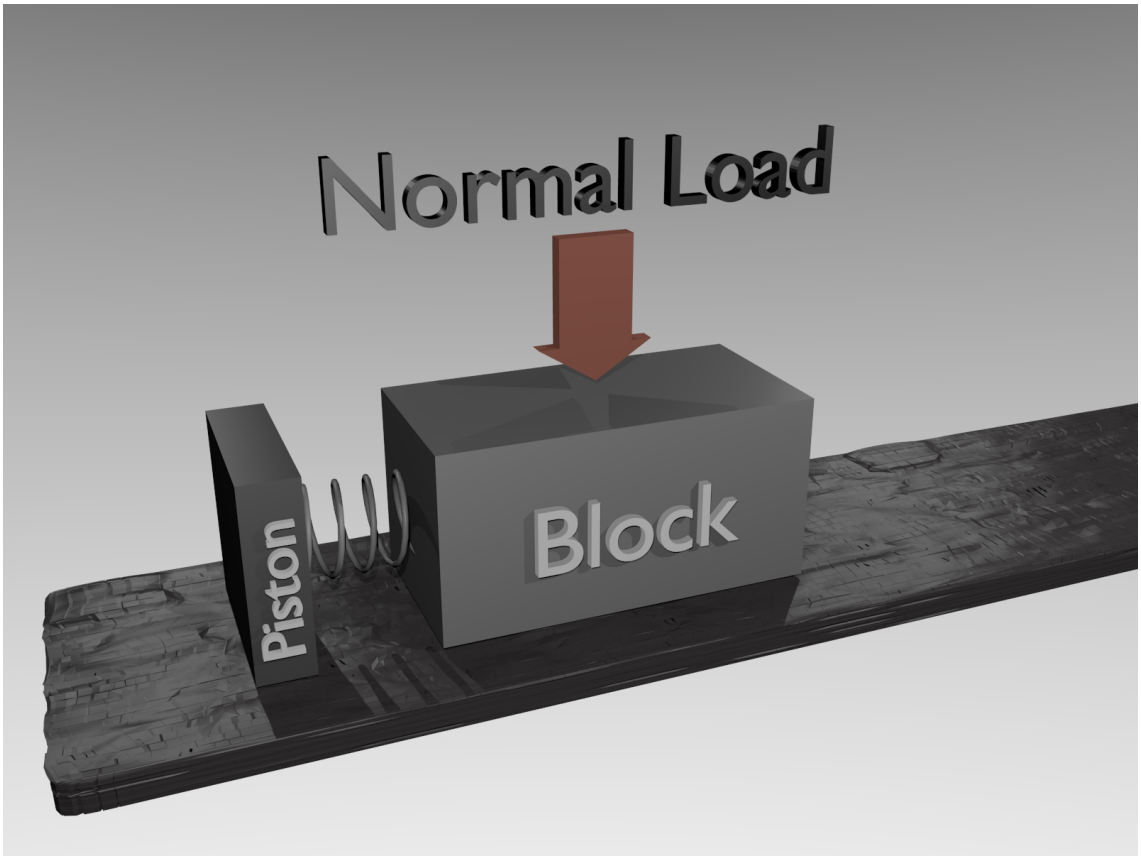

Figure 4.1: The slider

that each particle in the slider will then have a characteristic mass m_0 given by

$$m_0 = M/(N_x \times N_y \times N_z) \; . \tag{4.1}$$

The coordinates of a lattice point $\alpha \equiv (x, y, z)$, where $0 \leq x \leq N_x$, $0 \leq y \leq N_y$, $0 \leq z \leq N_z$. And $L_x = N_x l_0$, $L_y = N_y l_0$, $L_z = N_z l_0$. The elements in the slider are connected through (NN) nearest-neighbour and (NNN) nextnearest-neighbor with hookean springs in three-dimensions and viscous damping [16]. In the slider there are two such springs, k_1 for nearest-neighbour interactions, and the diagonal spring k_2 for nextnearest-neighbour interactions. The type of spring connecting neighbours i and j are determined by

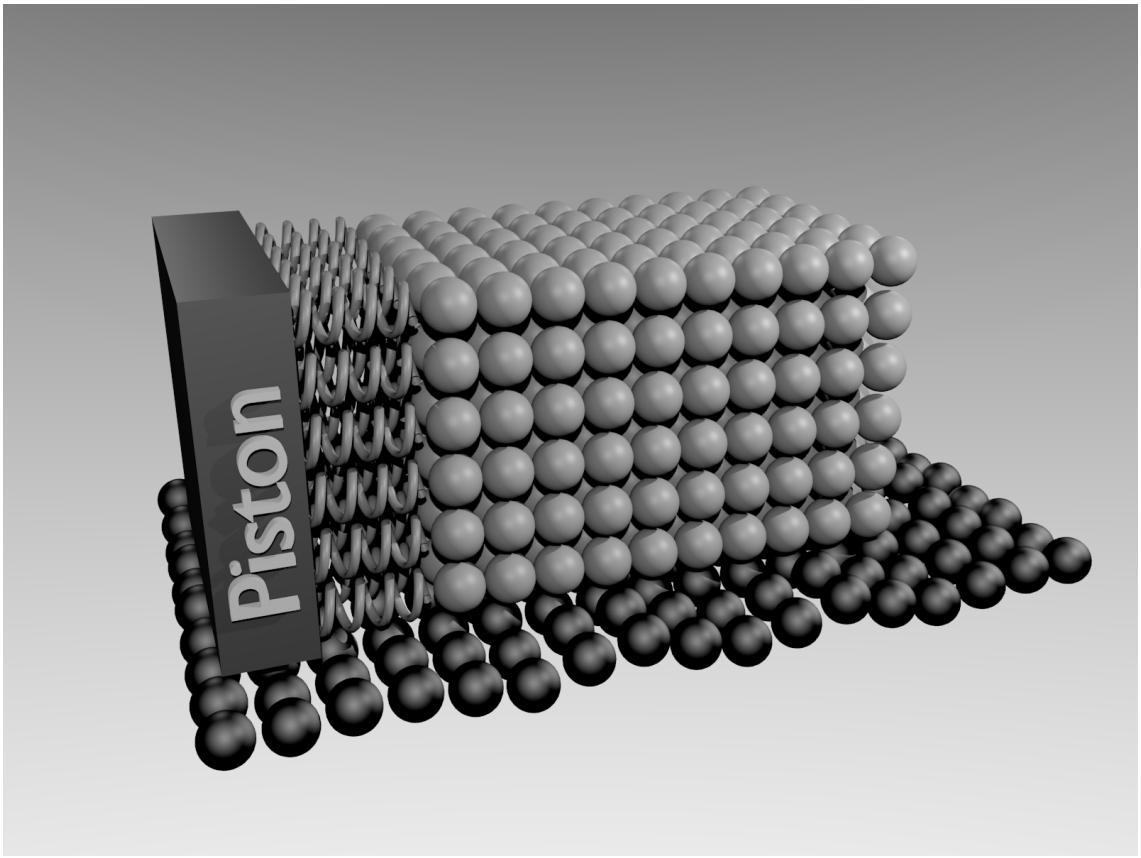

Figure 4.2: Discretized version of the slider

$$k_{ij} = \begin{cases} k_1, & \text{if } j \text{ is of type nearest-neighbour} \\ k_2, & \text{if } j \text{ is of type next nearest-neighbour} \\ 0, & \text{if } j \text{ is none of the above} \end{cases} \tag{4.2}$$

The diagonal springs detains the slider from falling over sideways and add shear elasticity to the system [17]. Further springs could be added for extra stability, but for my purpose the ones that already are available are enough. Contacts between the base and the slider and the piston and slider are given by k_b and k_w respectively. The values of these spring constants are set according to numerical criteria described in Chapter 6. The nearest-neighbour connections have an equilibrium length $eq_1 = l_0$ and the nextnearest-neighbour connections have an equilibrium length $eq_2 = \sqrt{2}l_0$ This implies that if there

are no internal or external forces acting on the slider it will have the same spacing between all elements in all directions.

4.3 Neighbour configurations

A typical element i in the slider can be connected to eight other elements in its own horizontal plane, in addition there are five more connections with other particles in each of the horizontal planes immediately above and below it. This totals a maximum number of eighteen possible neighbours for an element found whitin the slider. The corner elements in the slider have a maximum of 5 available neighbours within the slider. The force between two internal elements i and j (where $i \neq j$), found using Hooke's law is given by

$$\vec{F}_{int,ij} = k_{ij}(|\vec{r}_i - \vec{r}_j| - eq_{ij})\hat{\vec{r}}_{ij} \ , \tag{4.3}$$

where

$$\hat{\vec{r}}_{ij} = \vec{r}_{ij}/\left|\vec{r}_{ij}\right| \ , \tag{4.4}$$

where $\vec{r}_i$ and $\vec{r}_j$ are the respective positions of particles i and j. $\hat{\vec{r}}_{ij}$ is a unit vector pointing in the direction from i to j. In addition to the neighbours situated internally in the slider, each particle in the lowest plane of the block can have several neighbours in the base. Depictions of the various configurations can be seen in Figure 4.3 to Figure 4.7 at the end of this chapter.

4.3.1 Damping

All of the elements within the slider connected by springs are subject to a dissipative force. So, for a connection between elements i and j the term is given by

$$\vec{F}_{slider,ij} = -\eta_{ij} v_{ij} \ . \tag{4.5}$$

Where η_{ij} the coefficient of damping, and the damping force $\vec{F}_{slider,ij}$ is proportional to v_{ij} which is the relative velocity between element i and j. In order to gain in intuition about the behaviour of the system,let us examine the motion of a single particle connected to a spring attached to a rigid wall. The total force on a such a body with mass m connected to a spring with stiffness k is given by

$$\sum F_x = -kx - bv_x \ . \tag{4.6}$$

The additional term, $F = -bv$ is the same as the one described in equation above, where $v = dx/dt$ is the velocity and b is a constant that determines the amount of damping [22]. Applying Newton's second law to an object we get

$$-kx - b\frac{dx}{dt} = m\frac{d^2x}{dt^2} \ . \tag{4.7}$$

This differential equation describes the motion of the particle, where the solution is given by

$$x = Ae^{-(\eta/2m)t}\cos(\omega' t + \phi) \ . \tag{4.8}$$

A and ω' are respectively the amplitude and angular frequency of the oscillation(and decreases because the dissipative force). x is the position of the particle at time t. The angular frequency $\omega' = 2\pi f$, solving for the frequency f

$$f = \frac{1}{2\pi}\sqrt{\frac{k}{m} - \frac{\eta^2}{4m^2}} \ . \tag{4.9}$$

For a damped harmonic oscillator we have three possible modes of behaviour determined by the damping ratio ζ

- If $\zeta = 1$, this known as critical damping. A critically damped system will return to equilibrium without oscillating quicker than any other system. For a system that is critically damped, the frequency $f = 0$.

- If $\zeta > 1$, this known as overdamping. An overdamped system will return to equilibrium without oscillating but at a slower rate than a critically damped system. Greater values of ζ causes the return to equilibrium to be slower.

- If $\zeta < 1$, this known as underdamping. An underdamped system will oscillate with progressively smaller amplitude, while gradually returning to the equilibrium position.

Solving E9 4.9 for frequency $f = 0$ (critical damping) we find

$$\zeta = 1 = \frac{\eta}{\sqrt{2km}} \Rightarrow \eta = \sqrt{2km} \, . \tag{4.10}$$

I prefer the oscillations in the springs of my system to be underdamped, i.e I want to have $\zeta < 1$. This can be achieved by writing

$$\eta = q\eta_c \, , \tag{4.11}$$

where

$$\eta_c = \sqrt{2km} \, , \tag{4.12}$$

To model various degrees of underdamping I multiply η_c with a factor q where $0 \leq q \leq 1$, where q represents the degree of critical damping being applied. The reason want to have underdamping in our model so that we can simulate some of the vibrations that would take place in a realistic system. For the connections in the slider we may write above equation as

$$\eta_{ij} = q\eta_{c,ij} \, , \tag{4.13}$$

where

$$\eta_{c,ij} = \sqrt{2k_{ij}m_0} \, . \tag{4.14}$$

4.3.2 Spring stiffness

Because I want to be able to model various materials found in the real-world with different degrees of stiffness, it would be convenient to relate the central force springs with stiffness k_1 and k_2 to Young's modulus. For a slider discretized into a lattice with cells, it can be shown that the block only behaves as an isotropic elastic medium if and only if we have $k_2 = k_1/2$ [17]. Where k_1 is related to Young's Modulus E by

$$E = \frac{4k_1}{3l_0} \, . \tag{4.15}$$

Combining the condition that $k_2 = k_1/2$ and using above equation enables me to write k_{ij} between i and j

$$k_{ij} = \frac{3}{4} E_0 E_{ij} l_0 \, , \tag{4.16}$$

where E_0 is value chosen for my simulations, and E_{ij} is determined by

$$E_{ij} = \begin{cases} 1, & \text{if } j \text{ is of type nearest-neighbour} \\ 1/2, & \text{if } j \text{ is of type next nearest-neighbour} \\ 0, & \text{if } j \text{ is none of the above} \end{cases} \tag{4.17}$$

The defintions above are only valid if the springs are symmetric, i.e. their stiffnesses is the same under tensile or compressive stress [17]. Proceeding, we can incorporate the definition of Youngs Modulus E_0 and write Eq 4.5 as

$$\vec{F}_{int,ij} = \frac{3}{4} E_0 E_{ij} l_0 (|\vec{r}_i - \vec{r}_j| - eq_{ij}) \hat{\vec{r}}_{ij} \ . \tag{4.18}$$

4.4 The Base

The base being modeled is a rough surface extending along the x and y directions, with lengths B_x and B_y respectively. It is intended that the piston will push the slider along the x-direction, therefore I must make sure that $B_x >> L_x$ and $B_y > L_y$. Initially the base is modeled as collection of particles with regular spacing l_0 in all directions, forming a flat rectangular base described by the following relations

$$B_x = X l_0 \ , \tag{4.19}$$

where X is the number of particles along the x-direction and

$$B_y = Y l_0 \ , \tag{4.20}$$

where Y is the number of particles along the Y-direction.

There is no need to have a higher resolution for the elements in the base than in the slider, because then the slider would move past the gaps smaller than the slider particles with less interaction then intended for my studies. In other words, relative to the slider the base will be too smooth. To simulate the roughness a small random displacement (created by random number generator with a uniform Gaussian distribution) of between 5 and 10% of the length l_0 is applied in all to the x, y and z-coordinates of each element in the base. Intuitively, I displace the initially flat base randomly in all directions, creating a type of roughness possibly found in nature or a machined surface.

Because the base is considered to be much harder than slider-block, the particles in the base does not move at all during the simulations, i.e the base in non-deformable. Creating a deformable base with moving particles would also require considerable more work and testing then I can afford to spend time on. For example, modelling such a base would lead to a substantial increase in the time required for a simulation, several more parameters to keep track of and calibrate as well as even more restrictions for the range of parameters already in use.

4.5 The slider-base interaction

Particles in the base and the lowest horizontal plane of the slider come into contact when the slider moves along the base. I have chosen the lattice constant l_0 as the maximum distance allowed between a particle i in the slider and a particle j in the base to qualify them as being in contact. If this criteria is met and such connection is formed, the particles are connected to each other with a spring with stiffness k_b. Contacts between slider and base particles are commonly referred to as junctions, and at these points there acts a force $\vec{F}_{b,ij}$. In addition to the neighbours inside the block, a slider particle can be connected to several base elements at the same time. Initially my simulations only allows the contact-springs to be compressed. If a connected spring is stretched beyond the equilibrium length defined by $eq_b = l_0$, the contact is removed. This is the condition for geometric friction. Adhesion-effects like welding of junctions are also possible to simulate by allowing the spring to stretch. Alternatively I could have set the spring constant irreversibly zero if the force on a spring exceed a critical value, say F_c. The force acting between slider element i and base element j is given by

$$\vec{F}_{b,ij} = k_{b,ij}(|\vec{r}_i - \vec{r}_j| - eq_b)\hat{r}_{ij} \ , \tag{4.21}$$

where

$$k_{b,ij} = \begin{cases} k_{b,ij}, \text{if } |r_i - r_j| - eq_b < 0 \\ \\ 0, \text{if } |r_i - r_j| - eq_b > 0 \end{cases} \tag{4.22}$$

Since the base is non-deformable, forces exerted by the slider on the base are disregarded.

4.6 Slider-piston interaction

At the start of the simulation the block lies stationary on the substrate. The piston starts moving at a constant velocity v_w, causing it to compress the spring placed between the piston and slider. This spring has a stiffness given by the constant k_w. Therefore a force $\vec{F}_w$ will act on all the elements constituting the side of the slider at its trailing end. Thus, the area of the spring can be thought of as equal to area of slider's side facing it. As mentioned previously, the piston is unaffected by the slider's motion. The force on each relevant slider element is given by

$$\vec{F}_{w_i} = k_w max(x_w - x_i, 0) \,, \tag{4.23}$$

where x_w and x_i respectively are the horizontal-positions of the piston and slider-element being pushed. The above equation states that as long as piston is behind the trailing end of the slider, there will be a force acting on the slider from it, This force can only act in the positive direction because of its definition.

4.7 Normal Loading and gravity

In addition to all the forces described so far there are two more left. For a realistic system, there has to be a gravitational force causing the slider to push down on the base to create friction. As we have seen from the earliest friction-related experiments a variable normal load N has also been applied. The total weight of the slider can be calculated with

$$\vec{W} = N_x \times N_y \times N_z \times m_0 \times \vec{g} \,, \tag{4.24}$$

where N_x, N_y and N_z respectively are the number of spheres in the x,y and z direction of the slider. m_0 is the mass of a single sphere and $\vec{g}$ is the gravitational acceleration.

I have decided to model gravity as a constant force acting in the negative y-direction. To be able to simulate a variable normal load I could introduce some sort of separate mechanism such as adding an extra term in my force-calculations. However, in the spirit of keeping things simple I decided to incorporate the normal load into the gravity. So by adjusting my initial

value for gravity I can easily emulate the effects of an additional normal load. The normal load N can then be expressed as

$$\vec{W} = Nx \times Ny \times Nz \times m_0 \times \vec{g'} \,, \tag{4.25}$$

where $\vec{g'}$ is the modified value of the gravitational constant.

4.8 The equation of motion for the slider particles

The total force between a slider-element i and valid neighbour j can be found by adding up all the terms discussed earlier in this chapter for such a configuration. More precisely, I combine my previous equations which gives me the equation that needs to be implemented in my program

$$\begin{aligned} m\ddot{\vec{r}}_i = \frac{3}{4}E_0 l_0 \sum_j E_{ij}(|\vec{r}_i - \vec{r}_j| - eq_{ij})\hat{\vec{r}}_{ij} \\ - \sum_j \eta_{ij}(\dot{\vec{r}}_i - \dot{\vec{r}}_j) \\ + \sum_j k_{b,ij}(|r_i - r_j|)\hat{r}_{ij} + k_w max(x_w - x_i, 0) + m_0 g\hat{k} \end{aligned} \tag{4.26}$$

I tried taking things a step further by using non-dimensional definitions for some of the parameters in the expressions above in the form of system units. However, this lead to a great deal of confusion when deciding appropriate values, and created circular dependencies severely limiting my choice for the values of certain parameters. Therefore I prefer the clean and simple version in Eq 4.26.

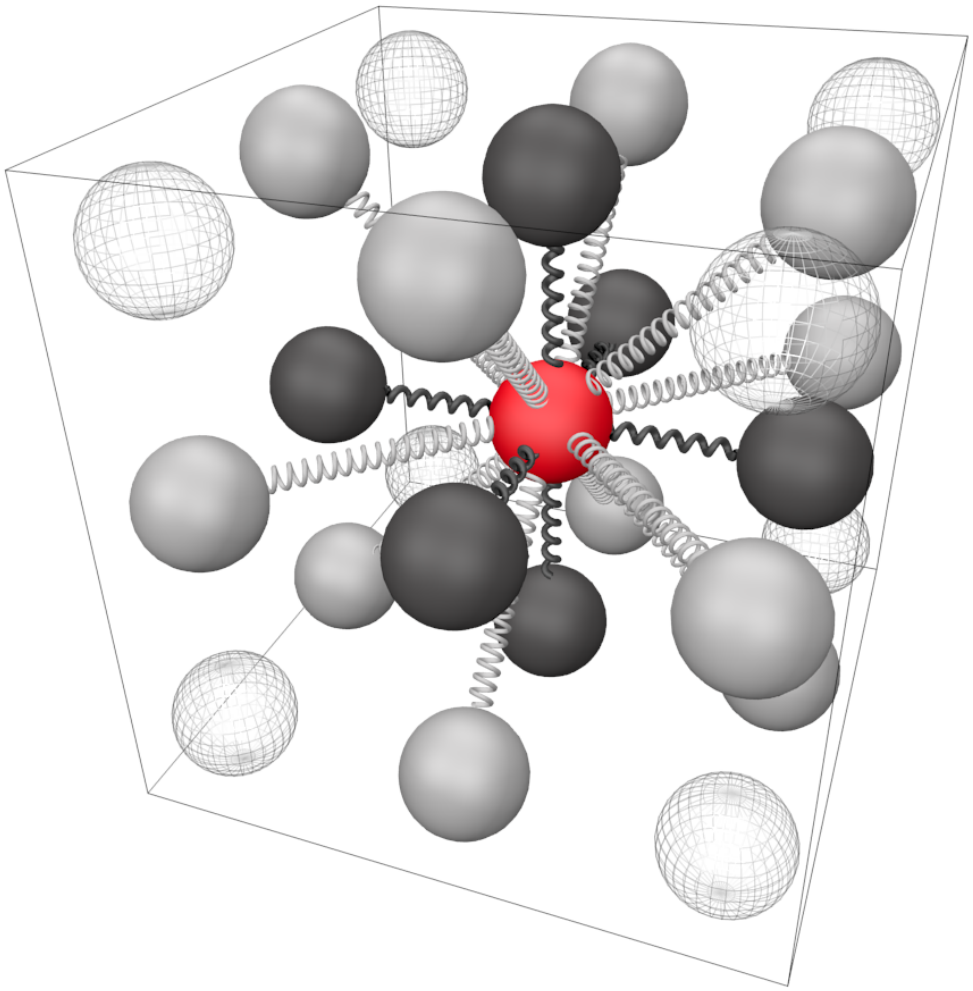

Figure 4.3: All possible neighbours within the block for a slider element

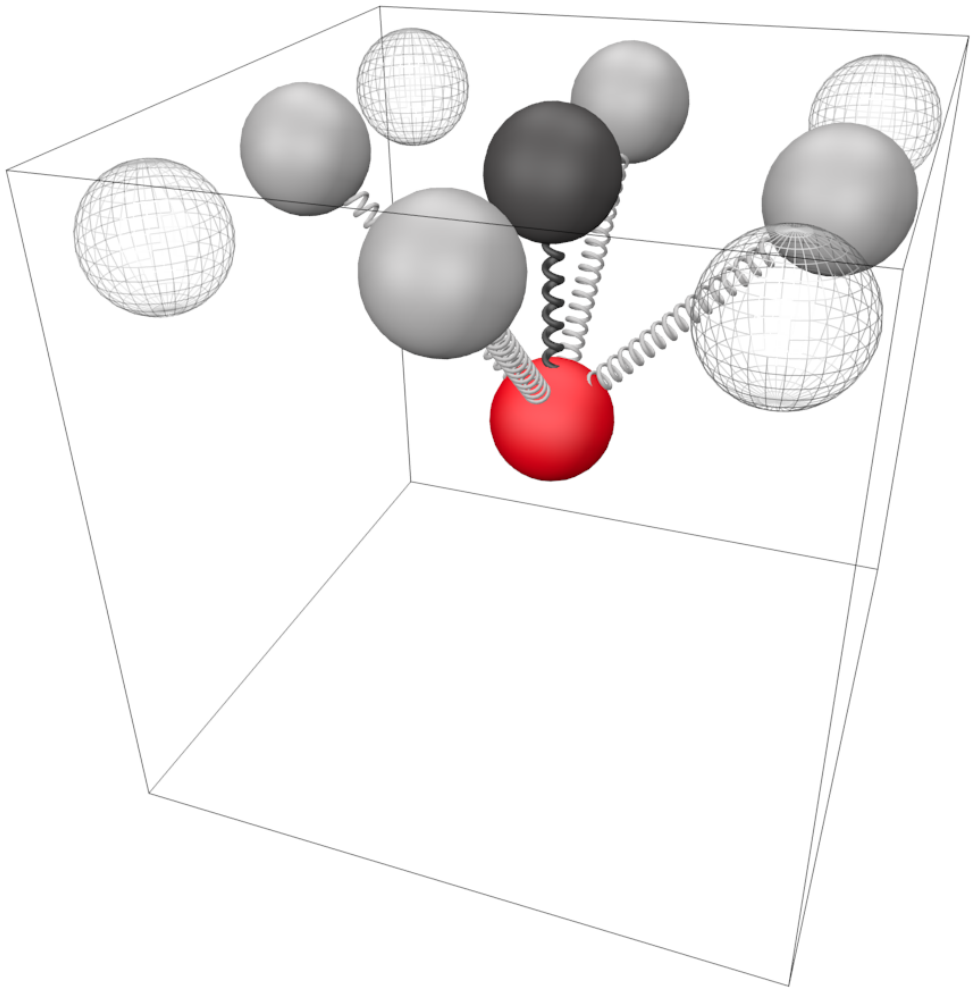

Figure 4.4: All possible neighbours in the plane above a slider element

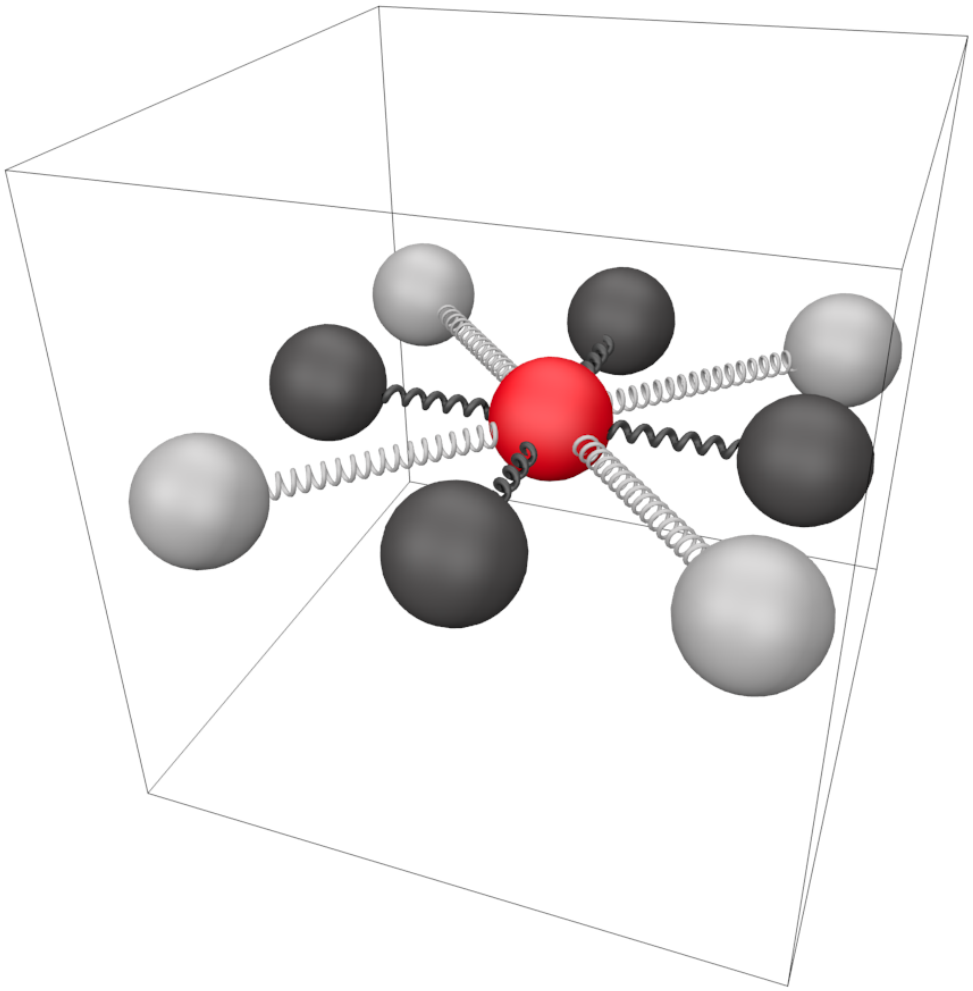

Figure 4.5: All possible neighbours in the plane same plane as a slider element

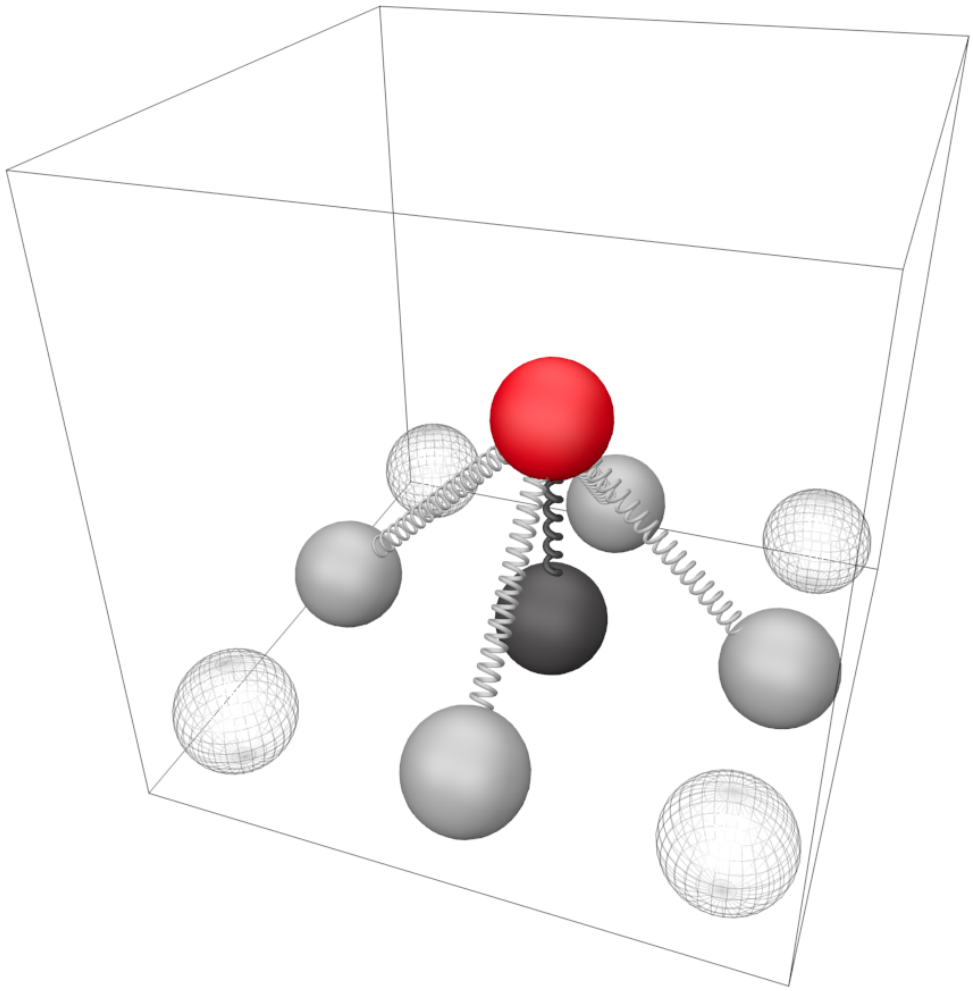

Figure 4.6: All possible neighbours in the plane below a slider element

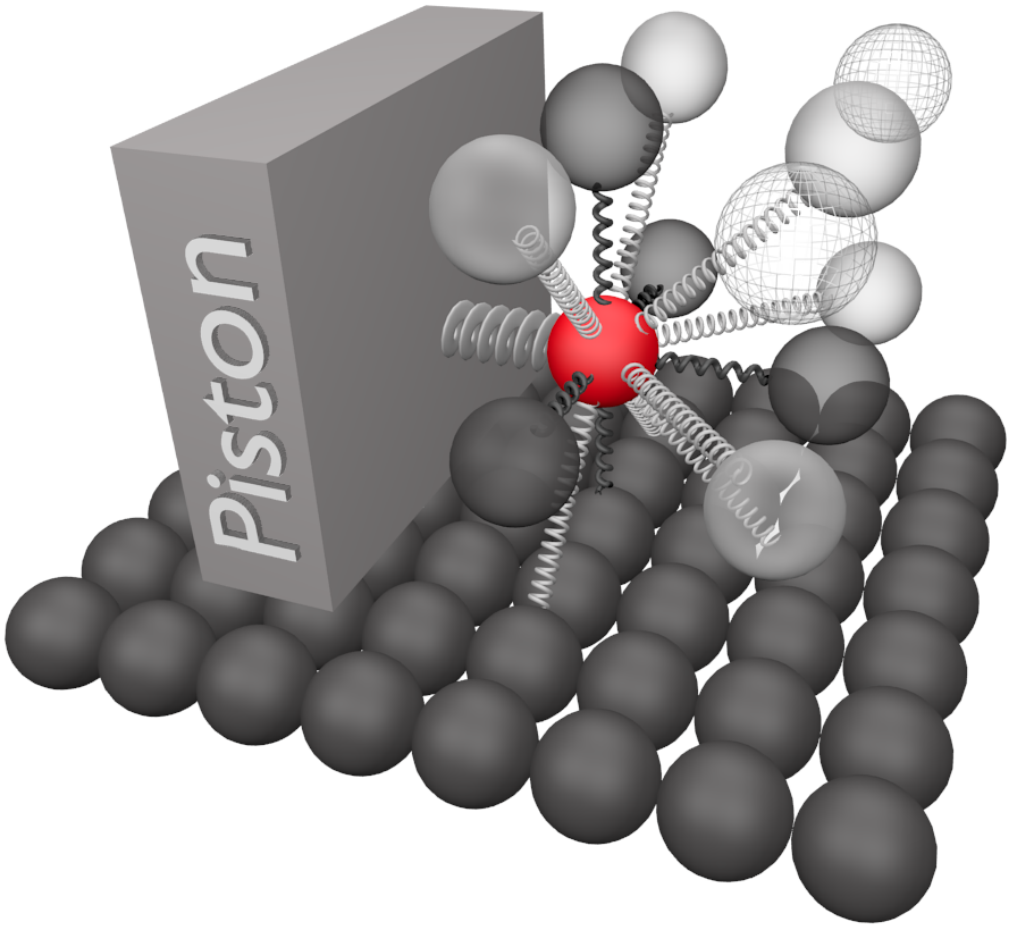

Figure 4.7: All possible types of interaction for a slider particle

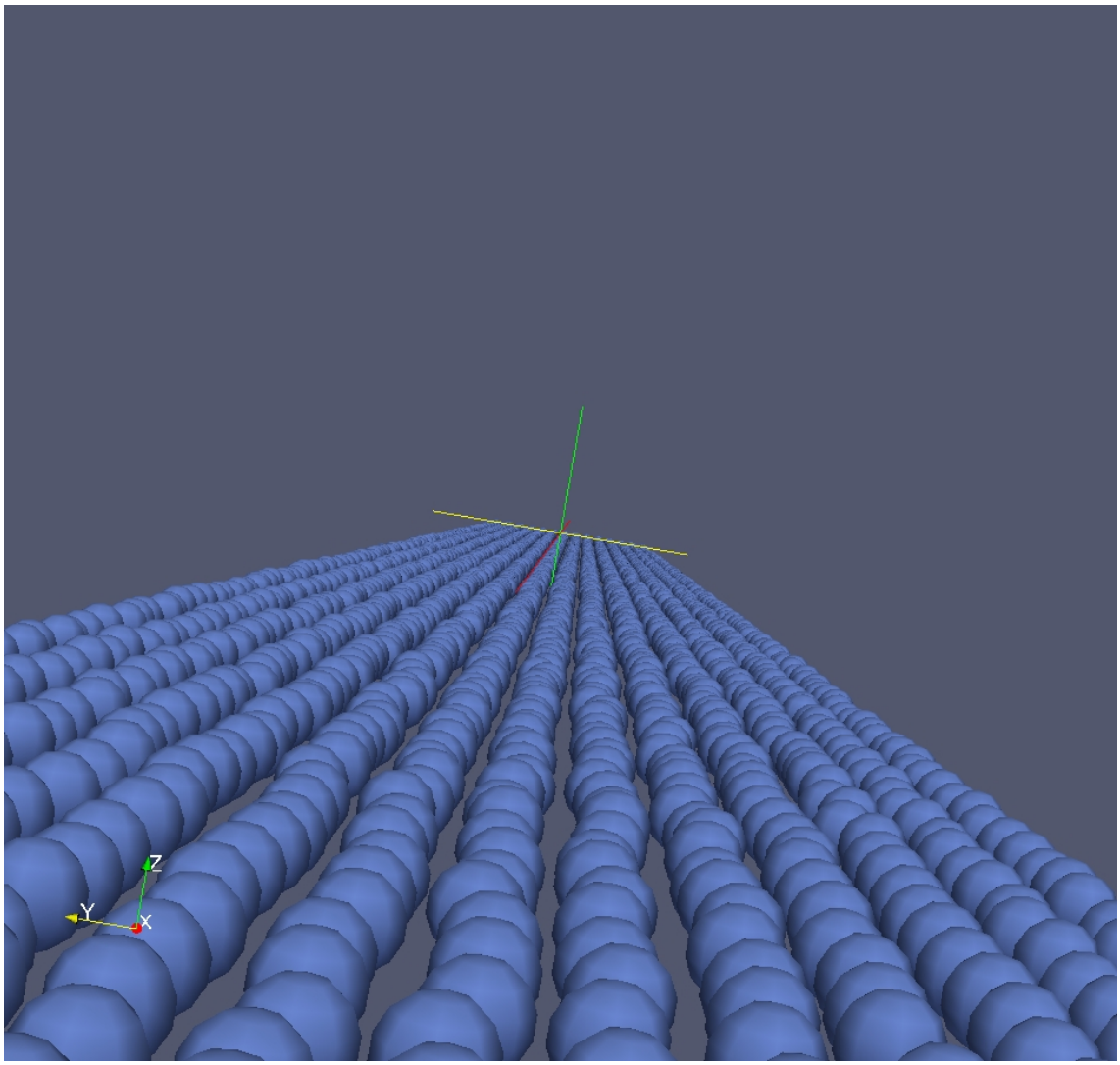

Figure 4.8: Screenshot from simulation showing disorder in the base

Chapter 5

The numerical setup

In the previous chapter we saw a detailed description of the physical model being simulated, the equations of motion needed to realize its implementation and conduct my measurements. In this chapter I present a breakdown and detailed discussion of the algorithms used in my program.

5.1 Algorithm

The list below contains the main elements of my program. In addition I created several help-functions only for debugging purposes and will therefore not be discussed any further.

- Initialize system
  - Create data structures
  - Initialize data structures
  - Find internal slider-neighbours
  - Find slider-neighbours in base
  - Find elements in trailing end slider wall
  - Open files
- Main Loop(iterate)
  - Calculate forces

  - Save image
  - Increment time
  - Move piston
  - Reset base neighbours
  - Find base neighbours
  - Collect data

- Close files
- Output parameter values

5.2 Initializing the system

Before any calculations can be done I need to do several other tasks. After declaring most of the variables and data structures required, I must initialize them with starting values. Because my program and its structure is relatively simple I mainly use global variables to avoid extremely long function calls. The initialization process involves defining values for all spring constants, Young's modulus, gravity, starting position of the piston, etc. During this phase I also build the slider and base, and position them accordingly. I have placed the piston at the origin ($x = 0$), therefore I place the slider at $x = l_0$. This creates an artificial equilibrium length (given by l_0) between them and has the added benefit minimizing the time needed to accelerate the slider. The slider is also moved in a distance $2l_0$ from the shorter edge of the base ($y = 0$). This is done to give more support to the slider so that it does not fall over the edge in case of sideways movement. The slider is also elevated a height l_0 above the base where $z = 0$. Before any force is applied to the slider it is uncompressed and has a regular grid-spacing.

```
int index = 0;
// Initialize x, y and z coordinates
for (int k = 0; k < z_dim; k++) {
    for (int j = 0; j < y_dim; j++) {
   for (int i = 0; i < x_dim; i++) {

index = i + (j*x_dim) + (x_dim*y_dim)*k;
```

```
position[index][0] = (i+1)*l_zero + 1.0*l_zero;  // x-coordinate
position[index][1] = (j+1)*l_zero + 2.0*l_zero;  // y-coordinate
position[index][2] = (k+1)*l_zero + 1.0*l_zero;  // z-coordinate
```

The code above is used for initializing the slider coordinates. The total force on the particles and their velocities are set in a similar fashion. For the base I only need to assign coordinate values to the particles, also in a similar manner as above, and apply a random displacement their values in order to simulate roughness. Because the base is stationary these values do not change, hence I do not need to keep track of the total force on them or their velocities. The total number of particles in the slider is calculated by

```
slider_size = (x_dim * y_dim * z_dim);
```

A particle with an index exceeding this value is flagged and treated as base particle. Once the slider has been placed on the substrate I can proceed to find all the particles that will be pushed directly by the piston and set an appropriate flag to distinguish them from other kinds of particles

```
void find_wall(){

double limit, min;
min = position[0][0];
limit = l_zero*0.25;

for (int i = 0; i <  slider_size; i++) {
       if (position[i][0] < min)
           { min = position[i][0];}
}


for (int i = 0; i <  slider_size; i++) {
       if ((position[i][0] - min) < limit)
            {particle_type[i] = -20;}
}

}
```

5.3 Initializing neighbours

Because I use NN and NNN, neighbours naturally can only be designated into one of these two categories. The program iterates stepwise through each element in the slider and calculates the distance between the current particle and the potential neighbour. If the potential neighbour lies within a specified distance, it is marked as a neighbour. This is costly computationally, but as this is performed only once this can be ignored. Failsafes are added in case of unforeseeable numerical behaviour rounding errors.

```
if (distance <= (1.0*l_zero)) //
{
neighbour      [i][neigh_site] = j;
force_const    [i][neigh_site] = k1;
damp_const     [i][neigh_site] = damping_1;
eq_length      [i][neigh_site] = distance;
//cout << "distance " << distance << endl;
neigh_site++;
}

else

if (distance > 1.0*l_zero && distance < sqrt2*l_zero*1.001) //
{
neighbour      [i][neigh_site] = j;
force_const    [i][neigh_site] = k2;
damp_const     [i][neigh_site] = damping_2;
eq_length      [i][neigh_site] = distance;
neigh_site++;
}
```

Locating neighbouring particles in the base is also done in a similar way. As mentioned this method is unfortunately very costly because you have to iterate through all the particles in the slider or base, so many operations are wasted. This of course slows the program down, and becomes very noticeable for larger systems. Ultimately, this sets limitations to the size of the system that can be modeled, i.e. both slider and base size.

It is often the case in programming that one has to choose between methods with varying degrees of efficiency, reliability, ease of implementation, etc. And in most cases some sort kind of trade-off will be involved. Because relatively small systems ($10 \times 10 \times 4$) appeared to give results reasonably close compared to the larger ones during various tests, I did not have to concern myself too much with computational efficiency.

5.4 Main Loop

The number of iterations in the main loop is given as command line argument to the program. Before entering the loop I have already once computed the neighbours for the slider particles that can be found in the base. This operation and every operation in the main loop is repeated a number of times determined by the input value. Although I have not moved the piston yet, there are other forces such as gravity, damping and so on that will cause displacement of the slider particles. The part of the program where I calculate the forces on the slider, is the actual implementation of Eq 4.26.

Because all the relevant neighbours have been found I can proceed to calculate the slider's new position, velocity and force. During the initial development of my program I used a Euler-Croemer scheme. Although efficient, it does not conserve energy. Therefore I settled on the velocity verlet algorithm to integrate Newton's equations of motion and find the new positions. The various verlet integrators are commonly used anywhere from MD-simulations to videogames. Some of the advantages this algorithm offers is its stability, efficiency and conservation of phase-space.

$$\vec{v}(t + \Delta t/2) = \vec{v}(t) + \frac{\vec{F}(t)}{2m}\Delta t, \tag{5.1}$$

$$\vec{r}(t + \Delta t) = \vec{r}(t) + \vec{v}(t + \Delta t/2)\Delta t, \tag{5.2}$$

$$\vec{v}(t + \Delta t) = \vec{v}(t + \Delta t/2) + \frac{\vec{F}(t + \Delta t)}{2m}\Delta t. \tag{5.3}$$

Where $\vec{r}(t)$, $\vec{v}(t)$ and $\vec{F}(t)$ respectively is the position, velocity and force for a particle i. The index i has been left out for brevity. By applying the above equations the values at the next time step for these vector-quantities can be calculated. Note that the forces are updated between Eq 5.2 and E.q 5.3.

5.4.1 Visualization

Because I want to be able to see the how the slider moves along the base, I needed to create a visual representation of the system. As the number of iterations required for a simulation was fairly large and the sliding velocity and time steps were comparatively small, there was no need to create a separate image for every time step. This is because the difference from one time frame to the next would not be very noticeable and also writing to disk is costly. The resulting images were later rendered in ParaView and used to create animations. By giving ParaView the coordinates to all of the particles in my system, Paraview was able to create snapshots of it. ParaView is a data analysis and visualization application allowing users to build visualizations and analyze their data interactively in 3D. The application is built on top of the Visualization Tool Kit (VTK) libraries that provide visualization services for data.

5.4.2 Increment time and move piston

The elapsed time had to be updated in the main loop, this was very easily done by keeping a single variable that would be increased by Δt for every iteration. Similarly, moving the piston was also very straightforward. The piston was implemented a single value representing the x-coordinate of the piston.

```
piston_x_coord = init_velocity*t;
```

Because the piston moves along at a constant rate $v_w = initvelocity$, all that had to be done to move it was to multiply by the elapsed time. It is important to understand that the motion of the piston will be unaffected by the slider. So even if the for some reason the slider does not move, the piston will move past it.

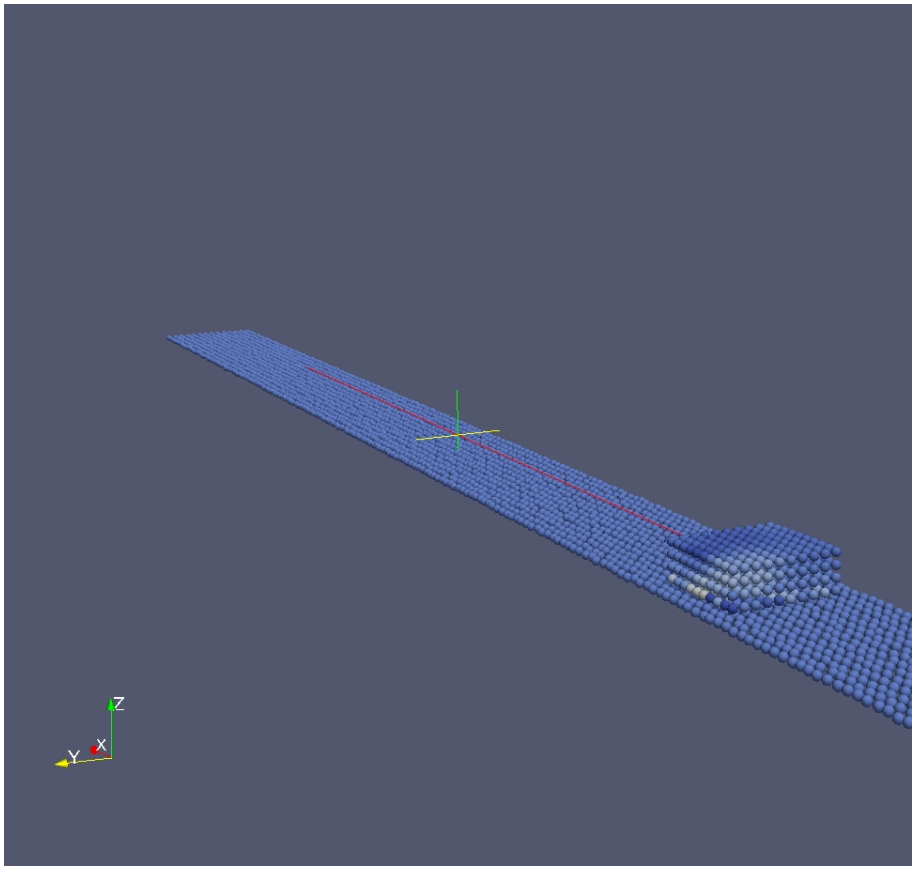

Figure 5.1: Screenshot from Paraview

5.4.3 Updating neighbours

Because I do not have permitted fracturing within the slider its internal neighbours naturally remains intact all the time. However as the slider moves along the track contacts are constantly broken and renewed between the substrate and the lowest horizontal plane of the slider. Therefore I have to reset all the connections between the slider and base from the previous time step that no longer exist whenever I update the time. If the distance between a slider-particle and a base-particle exceeds the set equilibrium length, the connection is reset, otherwise it is kept. To simulate adhesion effects I can allow for a greater stretching than the original equilibrium length.

```
if (distance > adhesion*eq_length[i][j]) {
reset connection
```

Where the variable adhesion gives the permitted stretching. For adhesion effects this variable is greater than 1.0, and if it is 1.0 we get regular geometric friction. Finding the new neighbours is also done by testing for a given distance between them. Keep in mind that I still have the old neighbours from the previous time step, so that I must make sure not to add these twice. Also to make sure that all the neighbours are found I multiply the equilibrium length with a number very close to 1, so that rounding errors are highly unlikely to exclude a valid neighbour.

An rough approximation for the total number of neighbours a slider-particle can have is estimated by assuming that for regular base the slider will have around 9 such neighbours. Adding this with the other possible neighbours gives roughly 30 possible neighbours.But for the sake of safety I set this value to 50 in my program. The indexing is divided into two groups. For an index value less the 20 it means that the particle is a slider-neighbour, for an index greater then this is is classified as a neighbour from the base. By doing this I am able to keep all neighbours within the same data-structure and at the same time distinguish what type of neighbour a particle is. This difference is important as the slider and base particles have different properties.

In my implementation there can only exist a connection between particles in the lowest horizontal-plane of the slider and base-particles. Therefore I only need to go through this lowest plane when updating the external neighbours of the slider. Because of the way in which I have indexed the particles in my system I only need to check the $N_X \times N_y$ elements constituting the lowest xy-plane of the slider (as opposed to $N_X \times N_y \times N_z$ particles).

5.4.4 Data collection

Along with the visual output produced by my program I also collect large amounts of numerical data for analysis and error checking. These values are dumped to disk at every iteration

- **The total force on the slider in the x-direction.**

Because the slider moves along the x-direction, this value is found by adding up all the x-components of force on the slider elements.

- **The velocity of the slider's center of mass**.
  This value is found by adding up all the x-components of velocity for the slider elements and dividing by the number of elements.

- **The position of the slider's center of mass.**
  This value is found by adding up all the x-coordinates of the slider elements and dividing by the number of elements.

- **The acceleration of the slider's center of mass.**
  This value is found by adding up all the x-components of $Force/m_0$ on the slider elements and dividing by the number of elements.

- **The slider's total energy.**
  This value by adding each slider element's kinetic and potential energy, which is generally written as $E_{total} = E_p + E_k = \frac{1}{2}kx^2 + \frac{1}{2}mv^2$. However, if particle i is particle j's neighbour it is also true that that particle j is particle i's neighbour. Therefore I must multiply E_p by 0.5 to compensate, otherwise I would add the contribution to E_p twice for the same interaction. So I my program I must use $E_{total} = E_p + E_k = \frac{1}{4}kx^2 + \frac{1}{2}mv^2$.

I calculate the additional quantities listed for each element in the lowest xy-plane of the slider and write them to disk every 10th time step. These are discussed further in Chapter 8.

- The dissipated energy which is given by

$$E_{diss} = \eta v_x \Delta x - \eta v_y \Delta y - \eta v_z \Delta z \ , \tag{5.4}$$

  where the index i is dropped for brevity. This value is derived from the work done by the viscous dissipative forces in the system.

- The absolute velocity-field(i.e. the absolute value of particle i's velocity)

- The normal-force F_{z_i} on particle i.

- The shear-force F_{x_i} on particle i.

- The height-field z_i (i.e. the particle i's height relative to the z-axis)
- The contact-field(i.e. the total number of neighbours particle i has in the base)

Chapter 6

Calibration of parameters

In the preceding chapter we took a look at the implementation of the model. Now it is time talk about the parameters in the actual program. In this chapter I will discuss and justify my selection of parameters and their chosen values. I have decided to define my system by two main parameters that I choose values for, Young's Modulus E_0 and the mass density ρ of the material that the slider is made of. Most of the other values for the remaining parameters follow either directly or indirectly from these two choices. Nevertheless, this was far from a trivial task and required a large amount of time to find the right values. Determining reasonable values for the parameters involved making sure the imposed constraints were kept combined with educated guessing.

6.1 Young's Modulus

Ideally I would like to have a real world value for E_0 and ρ , but unfortunately this does not necessarily match with my simulation and the associated numerical criteria discussed previously and further on. That is, I want the mechanical characteristics of the simulated object match the mechanical characteristics of real materials. I found during my tests for various values realistic values of E_0 that if it was too low, the slider would be highly unstable and deform far too easily compared to how such a block would respond in reality to the same actions.

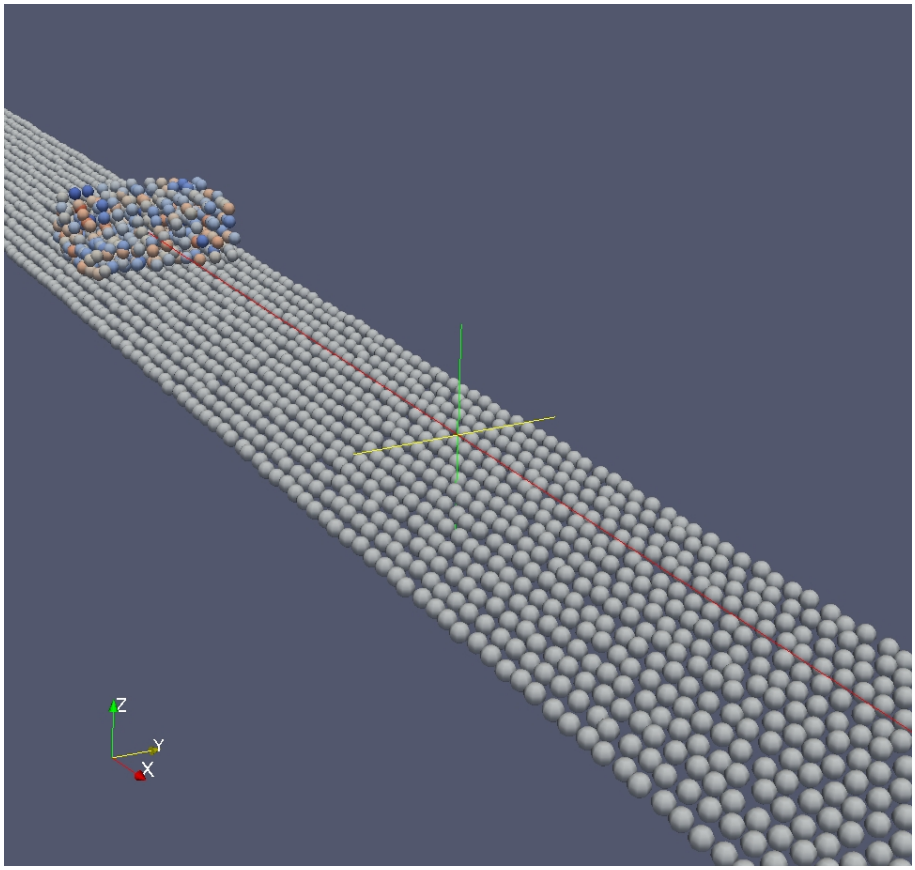

Figure 6.1: Deformation of the block during sliding

By studying the animations created in Paraview I concluded that a minimum value for Young's Modulus in my simulation is $E_0 = 1.0 \times 10^8 Pa$ if I want to avoid the anomalous behaviour illustrated in Figure 6.1 where the slider is deformed. Although I want the material to be rigid, I also need to keep to value of E_0 as low as possible. The reason for this is described later in this section.

6.1.1 Base spring k_b

We know from equations 4.16 and 4.17 that

$$k_1 = \frac{3}{4} E_0 2 l_0 \tag{6.1}$$

Because I want a fairly rigid base with very little deformation in the springs I must set k_b very close or equal to k_1 for this to be possible (since the value of k_1 already is set relatively low). So I get the following relation

$$0.9k_1 \leq k_b \leq k_1 \tag{6.2}$$

If the weight of each vertical column of the slider is supported by one base spring each

$$\frac{Mg}{N_x N_y k_b eq_b} = \Delta x, \tag{6.3}$$

each spring with stiffness k_b will experience a deformation Δx. eq_b is the equilibrium length for such a base spring. From the above equation I get the following constraint for Δx

$$\frac{Mg}{N_x N_y k_b eq_b} = \frac{N_x N_y N_z m_0 g}{N_x N_y k_b eq_b} = \frac{N_z m_0 g}{k_b eq_b} = \Delta x, \tag{6.4}$$

where the maximum allowed deformation is

$$\Delta x \leq eq_b 0.1 \tag{6.5}$$

6.1.2 Piston spring k_w

The spring between the slider and the wall has a stiffness k_w. Because I do not want to waste too much time accelerating the block I chose to set the value of this spring

$$0.9k_1 \leq k_w \leq k_1 \tag{6.6}$$

Having a spring which is too soft would cause the response of the slider to the wall's movement be relatively slow.

6.2 Mass density ρ

Because I used the value of the elasticity modulus for PMMA as a starting point, I also use its value for mass density as a starting point for my choice of ρ. I proceed to tweak this value for my system.

$$m_0 = \frac{M}{N} = \frac{10kg}{4000} = 0.5g = 0.5 \times 10^{-3}kg \tag{6.7}$$

6.3 Time step Δt

There are several things to keep in mind when choosing a value for my time step Δt. Since the springs obey Hooke's law I must make sure that a complete oscillation is resolved by a reasonable amount of time steps.

$$x(t) = \cos(\omega t) \tag{6.8}$$

where at the smallest scale an oscillation in my system is defined by

$$\omega = \sqrt{\frac{k_1}{m_0}} \tag{6.9}$$

because k_1 is the stiffest spring and thus oscillates fastest of all springs in the system, and m_0 is the mass attached to it.

$$\tau = \sqrt{\frac{m_0}{k_1} = \frac{1}{\omega}} \tag{6.10}$$

A complete oscillation is described by so if $\tau \approx 5\Delta t$

$$t = 2\pi\tau = 2\pi 5 \approx 30 \tag{6.11}$$

This means a complete oscillation will take about , $t = \Delta t^{30}$

6.4 Piston velocity v_w

As my title of my indicates, the simulations are conducted at low sliding velocities. But what exactly is a low sliding velocity? For my simulation I have defined a low sliding velocity as

$$v_w << l_0\tau \tag{6.12}$$

That is, the piston should move at a velocity such that the number of oscillations completed over the distance l_0 Don't want the slider to tip forward or lose contact with the base.

The sliding velocity needs to sufficiently small so that the interesting dynamics taking place in the interface between substrate and the base of the slider. At the same time I don't want for the simulation to take excessively long. At low sliding velocities, the temperature dependent effects related to friction can safely be disregarded. The majority of the simulation time is spent writing results to disc. The difference in simulation time needed was noticable when such processes were turned off, or kept to low number. The value of the sliding velocity v_w is the velocity at which the piston moves along the base. I also discovered when using a too high sliding velocity that, aside from violating the constraints the slider would have a tendency to lose contact with the base at the trailing end and tilt forward along the sliding direction.

The motion of the entire slider can be characterized by the mass-centers velocity v_{cm}. Because of relative motion within the slider, each particle in the slider also has an individual velocity. Alternatively

$$v_w \Delta t << l_0 \tag{6.13}$$

6.5 Time step Δt

In order to have a stable system I must have a small value for the time step Δt. However, I must keep in mind that I cannot just chose an arbitrarily small value. The time step at time t_n after n time steps is

$$t_n = n\Delta t, \tag{6.14}$$

the smaller Δt becomes, the larger n must be to simulate a given time t. The larger the system becomes, the more physical time is needed for a simulation.

The time-step also sets limitations to the size of the slider when simulation time is taken into account. I need to keep ρ relative large compared to E_0. This is because m_0 and k_1 depend on ρ and E_0 respectively.

$$\Delta t << \tau = \sqrt{\frac{m_0}{k_1}}, \tag{6.15}$$

Now we see the reason for my earlier choices. The larger E_0 and therefore k_1 is, the smaller I have to keep Δt. Similarly, the larger ρ and therefore m_0 is,

the greater I can set Δt. So one can see that this is all a very delicate balance between several parameters, and not as trivial a task as it may appear at first. One sees that by decreasing k_1 the possibility to have a larger time-step is there.

6.6 Gravity

Seeing as I had to depart from my original intentions of having realistic values for my parameters I chose to define my value for gravity g in terms of the already selected values, as choosing a real-value g would not make much sense at this juncture. Thus, I have the following relation to help me decide my choice for g.

The force experienced by a spring k_1 is For a block of mass M the amount of compression Δx experienced by $N_x N_y$ springs of type k_b with equilibrium length k_b supporting its weight can be written

$$\frac{Mg}{N_x N_y k_1 eq_b} = \Delta x, \tag{6.16}$$

using $M = N_x N_y N_z m_0$, solving for g

$$g = -k_b \Delta x eq_b)/(m_0 N_x) \tag{6.17}$$

where Δx is the amount of deformation in a spring with stiffness k_b and equilibrium length eq_b. The value for $Deltax$ is

$$\Delta x \leq 0.1 eq_b \tag{6.18}$$

so the maximum value I can use for g is

$$g_{max} = -\frac{k_b 0.1 eq_b}{m_0 N_x} \tag{6.19}$$

Because the base is supposed to be essentially non-deformable I allow no more than 10% deformation due to gravity and normal load. My definition becomes slightly problematic when it comes the transition between only gravity and the combination of gravity and normal loading. Nevertheless, this is an issue which really is unimportant for my project and thus I will not dwell anymore on this point.

6.7 Base and slider size

The size of the base needs to be at least three times the length of the slider because I assume that by sliding this distance at a steady velocity I will be able to detect repeating patterns. Additionally I need to take into consideration that the slider will need some time to reach a steady velocity, so I ended up with a base about five times the length of the slider. This might seem like nitpicking, but one has to consider the fact that every particle in the bottom of the slider tests each particle in the base for a possible neighbour for each time-step. One realizes that each extra neighbour increases the overhead significantly enough to consider this carefully. The base also needs to be slightly broader than the slider so that it does not fall over the edge in case of a slight sideways movement. It is fairly safe to assume that there will not be much sideways movement, so breadth of the base only needs to be slightly wider than the slider itself.

After trying out various dimensions for the slider I finally settled for $L_x = 10, L_y = 10, L_z = 4$. I found that a larger slider did not improve the results significantly enough, but only required more valuable simulation time and disk space. Another important thing to keep in mind when choosing the system size was that if the slider was too tall relative to its breadth and width it would easily tip over its edge when set in motion.

Chapter 7

Testing

In this chapter I briefly discuss some of the ways I tested my program along with some of the challenges I faced while creating the program.

7.1 Tests

The testing phase of the program was a continuous process that had to be repeated for any significant changes made to my code, be it a different algorithm or a new set of parameters. Some of the basic tests I performed were

- **Gravity**
  By placing the slider at a height greater than its own above the base (and turning off the piston) I was able to check if the slider would fall down and how much time this would take. This was also useful to see if the slider would stop at the base or continue to fall through the base. A screenshot of the slider being dropped can be seen in Figure 7.1.

- **Impact between slider and piston**
  In the case of a perfectly inelastic collision where one object(the piston) has a mass much greater than the other (the slider), the slider will achieve a velocity twice the value of the piston's velocity, provided the slider was not moving before the impact. I achieved these conditions by turning off all dissipative forces, gravitation and removing the base. A plot from one of my tests is seen in Figure 7.2.

- **Counting neighbours.**
  Perhaps the most time consuming part of the already time consuming testing phase was making sure that the all the correct particles were connected to each other. This involved reading through several long lists of numbers and drawing numerous diagrams for checking purposes. I wanted to make sure that the program would function correctly for a wide range of system sizes, not just one.

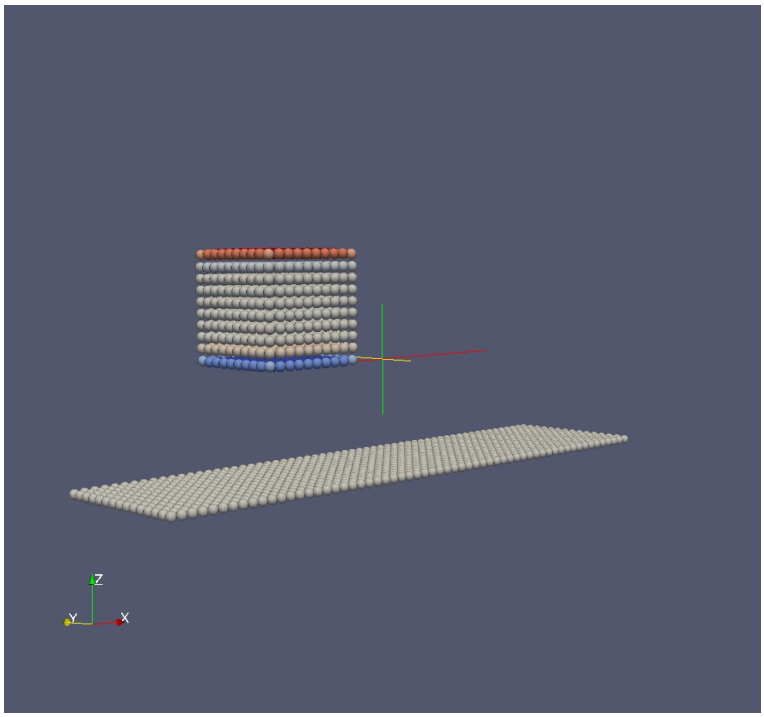

Figure 7.1: Slider during free-fall

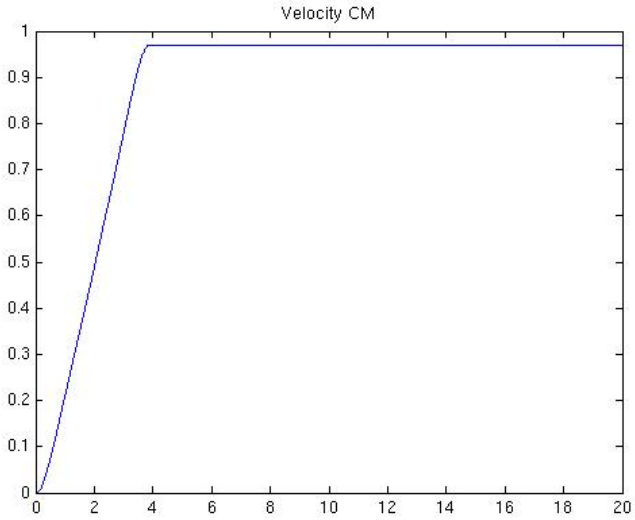

Figure 7.2: Velocity for center of mass without any base, gravity and dissipation

Chapter 8

Results for sliding at steady velocity

After completing extensive tests on my program, I continue with the simulations needed to produce the necessary data. I am looking to uncover how the base of the slider interacts with the substrate as it is pushed along the track at a steady velocity. Is the motion smooth, does all the particles dissipate the same amount of energy and experience the same amount of force on them? These are some of the questions I hope to be able to answer by the completion of this phase. There are several measures for quantifying the overall motion of the slider, but not all of them are equally useful. By comparing the various measures such as normal force, shear force, acceleration, etc, I expect to find out more about the interaction.

Because the surface is rough I do not expect the motion of the slider to be completely smooth, even though it appeared so from the animations I created to see that the system behaves correctly. This expectation also makes sense with regard to the MCI theory (where local contact populations are broken and replaced continuously). I also assume that the front of the slider will experience the most dissipation during sliding. This is because when the slider is pushed at the trailing end it will cause parts of the rear end to be slightly lifted above the base, thus having less overall contact with the base. However, it is also possible that this effect is negligible since the sliding speed is relatively low.

8.1 Motion of the slider

As one can see from Figure 8.1, the slider is initially motionless at the start of the simulation. When the piston starts pushing it forward, the slider experiences a large accelerating force seen in Figure 8.2. The slider speeds up gradually until the sliding velocity becomes increasingly steady with only minor fluctuations ($v_p \approx v_{cm}$) at around 2 seconds. The slider experiences the greatest acceleration upon the first impact with the piston as seen in Figure 8.2. After the initial push the slider has a series of smaller impacts with the piston at progressively smaller time intervals. When the sliding velocity has become stable enough, the position of the mass center increases more or less in a linear fashion as seen in Figure 8.3 and the variations in the slider's energy decreases as seen in Figure 8.4.

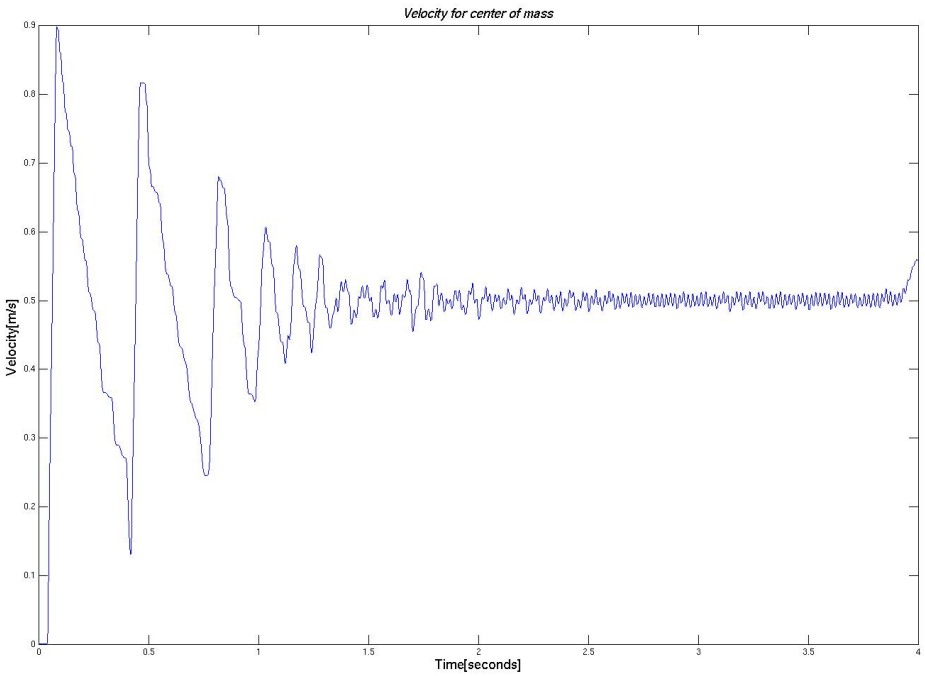

Figure 8.1: Velocity for center of mass

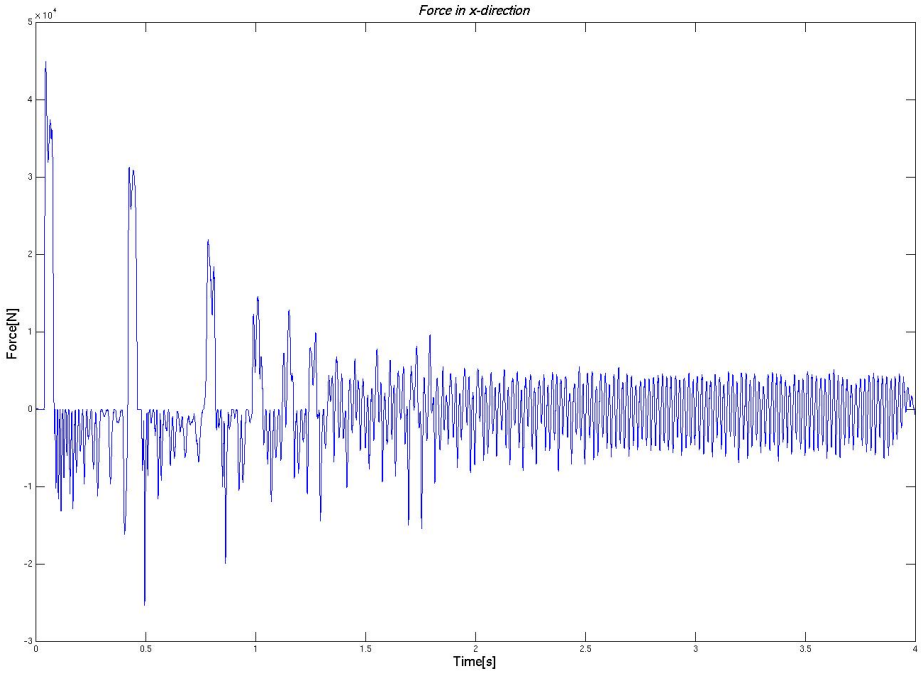

Figure 8.2: Force on slider

8.2 Analysis of motion

Because I am looking at what takes place at a steady velocity, I need not concern myself with events that take place before such a velocity is reached. Examining Figure 8.1 closer, I see that the fluctuations for the mass center velocity is "semi-periodic". A closer view of such a "periods" is seen in Figure 8.5. I will analyze a series of such periods in the following section, so that I can find out what sort of events take place during this time.

8.2.1 Comments

Since the behaviour is semi-periodic it does not matter where I choose the starting point for my investigation, as long as I stay within the region where this type of behaviour occurs. Part of the reason for the periods being slightly different is that the base is irregular. I assume that pattern would appear

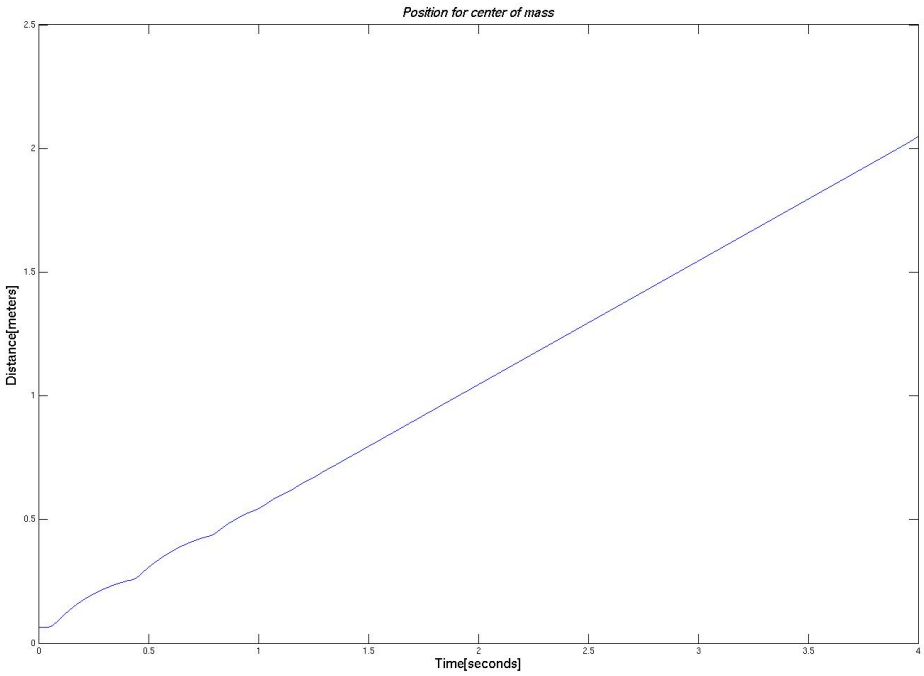

Figure 8.3: Position of center of mass

more consistent if the base completely flat.

Figure 8.6 shows the different measures at time $t = 2.0$. It is apparent that the change in velocity is stable around this point and oscillates around the driving velocity for the piston. The force on the slider from the piston fluctuates at a much higher rate than any of the other measures. The rapid oscillations observed in the force on the slider can be interpreted as a series of repeating impacts between the slider and the piston. At this point the force on the slider is negative indicating that slider is slowing down. One can also see that although the force is negative, it is increasing and therefore there is a corresponding increase in the velocity impending further on.

The value of the velocity field towards the front of the slider is lower than the velocity field at the back. This shows that the all parts of the slider does not move simultaneously and with equal velocity.

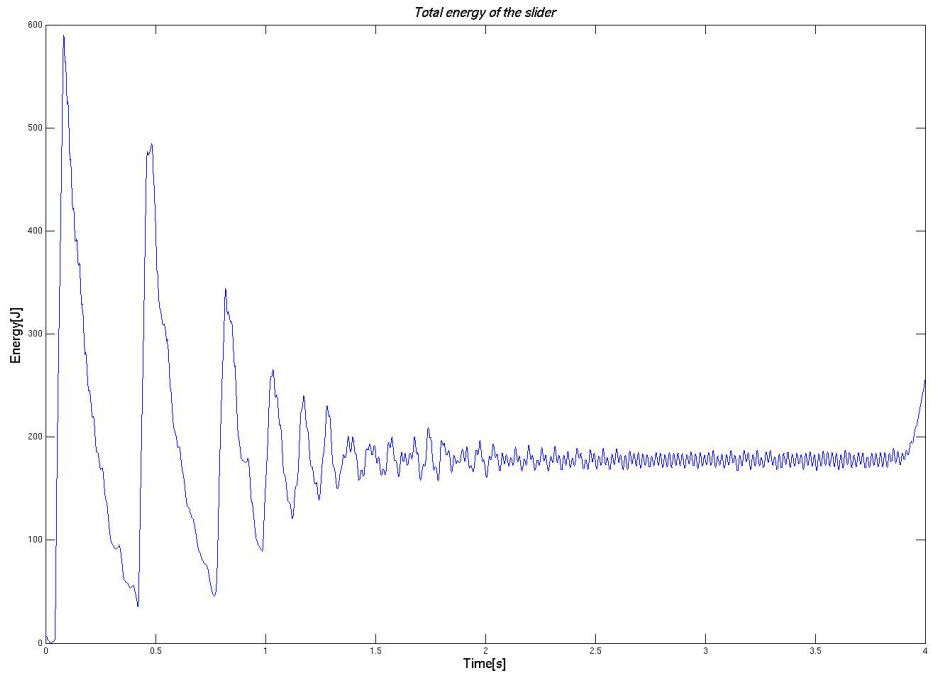

Figure 8.4: Energy of slider

In the current time-frame the number of contacts between the slider and base are relatively low hence only a small number of particles experience shear and normal forces. This also makes sense with the amount of dissipation and the regions where it occurs having the highest values. Measures at an earlier time shows that the number of contacts were even less than the present number. Moving forward in time, the results shows that the number of contacts increase gradually. This is again followed by a decrease, only to repeat the same cycle over again.

The way in which I have measured the dissipation is by taking the difference between the same number of time-steps backward and forward in time around the specific point I am looking at. The amount of dissipation taking place over an interval is dependent on the number of contacts, where a low number of contacts results in a low amount of dissipation. And a high num-

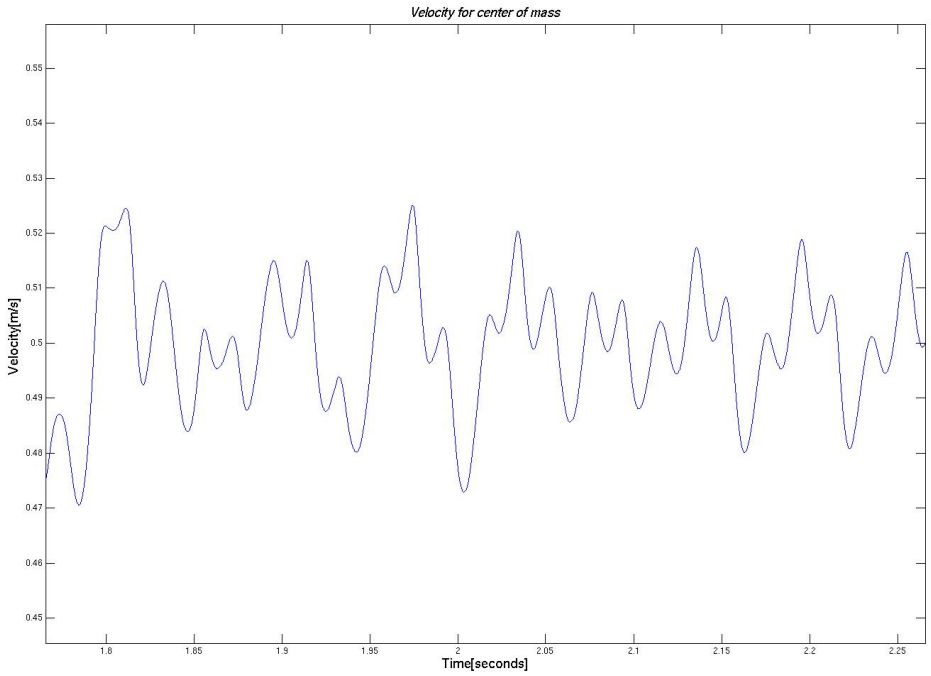

Figure 8.5: Velocity for center of mass

ber of contacts results in a high amount of dissipation. For different points in time areas with a similar number of contacts, the amount of dissipation is comparable.

Although there is a connection between the number of points where the normal and shear force are acting the variation in their values seem to have a lower correlation. The normal force does not seem to fluctuate as much as shear force. The force on the slider is the value that varies the most during a period. The slider does not move equally at all points, possibly due to the roughness in the base. Variation in contact population take place over several cycles.

At time $t_2 = 2.005$ in Figure 8.7 we can observe some changes from $t_1 = 2.005$ in Figure 8.6. The mass center velocity has started to increase again as a result of the increasing force on the slider. A slight variation in

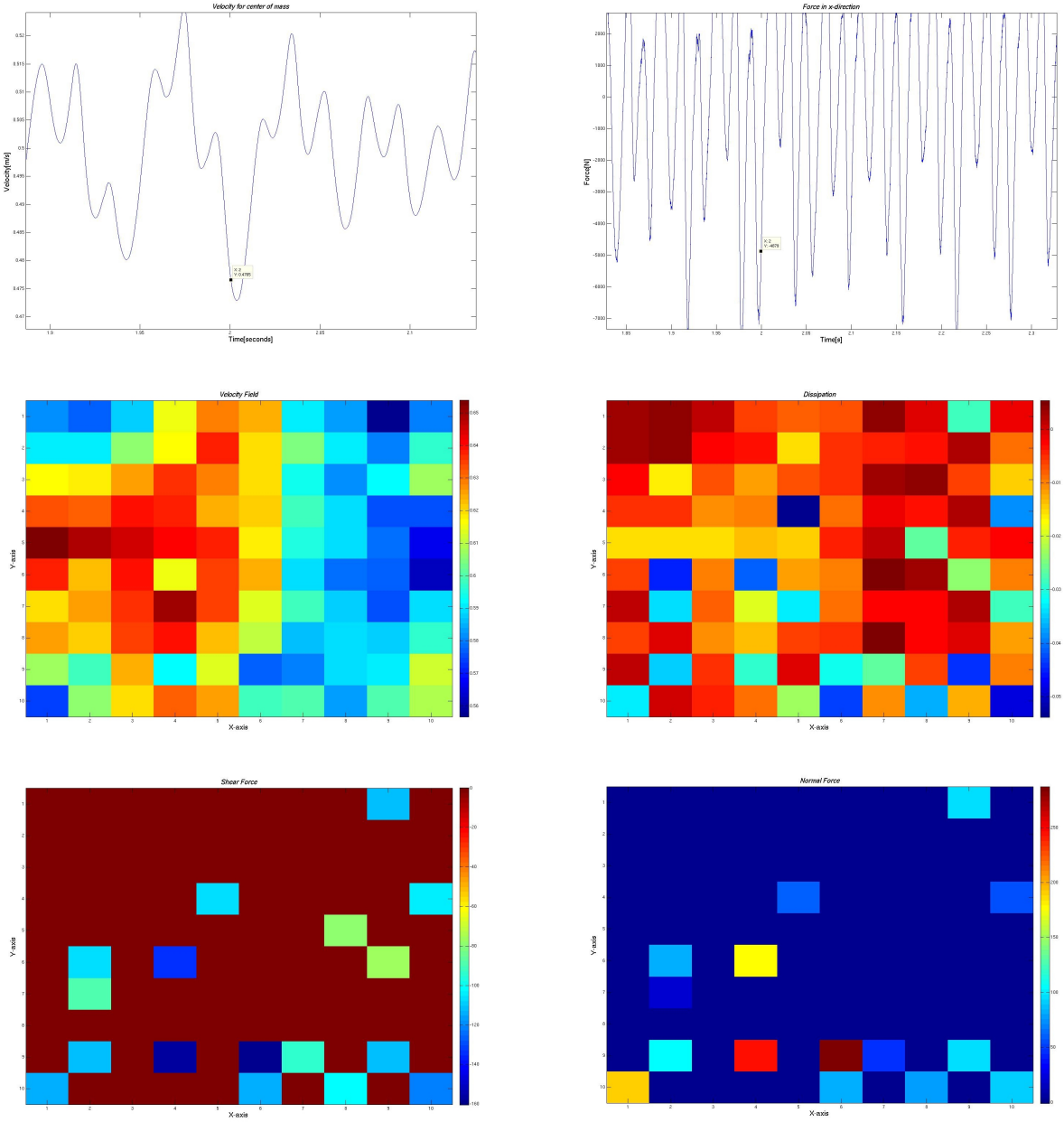

Figure 8.6: System at $t_1 = 2.000$ seconds

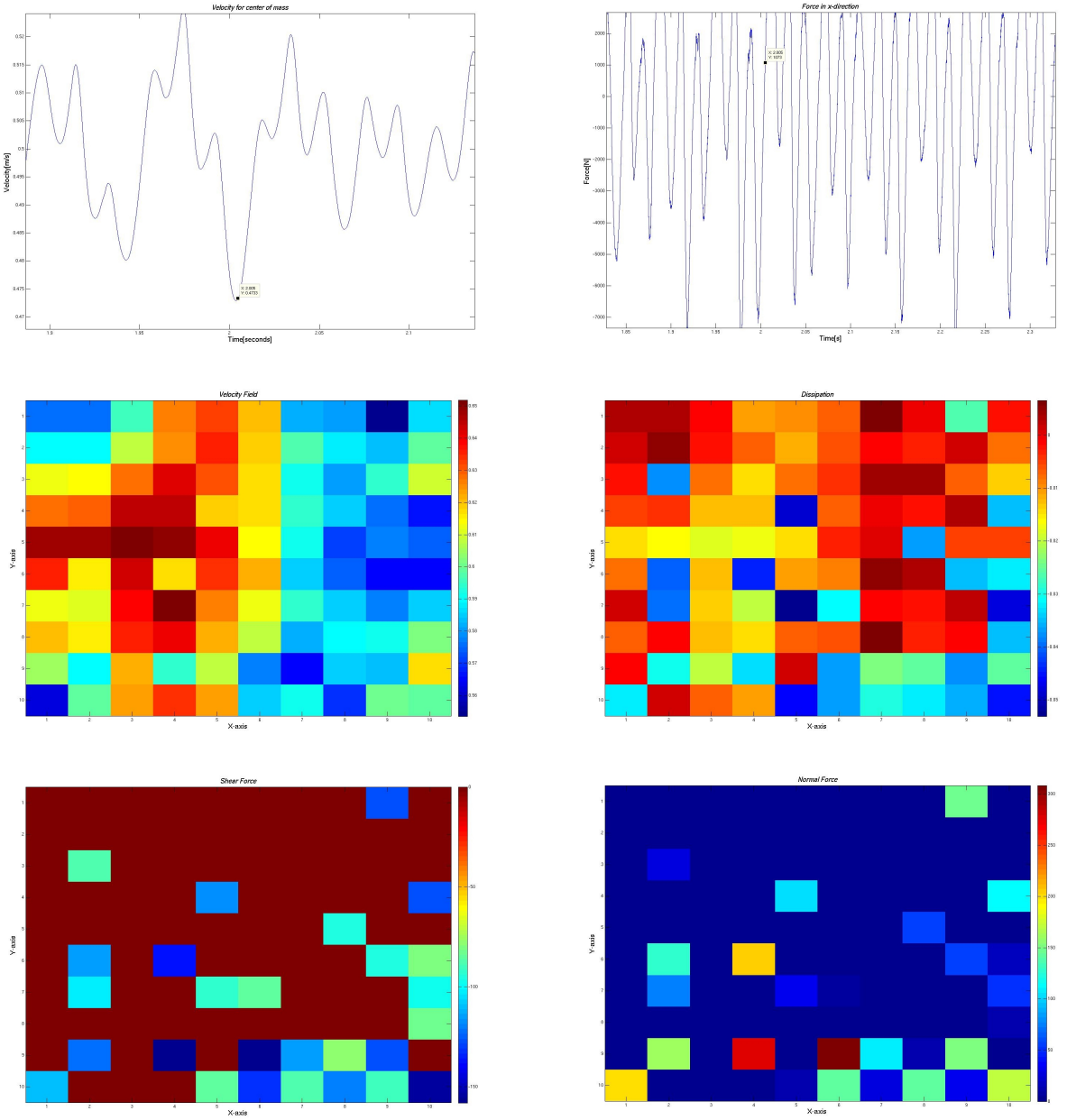

Figure 8.7: System at $t_2 = 2.005$ seconds

the velocity field also indicates this. One can also see from the change in the velocity field that not all the particles necessarily experience the same amount of relative shift in their velocity as neighbouring particles do.

We can also see by comparing Figure 8.7 and 8.6 that there is an increase in the number of contacts, as well as an increase in the shear and normal forces. The difference in time between the images in Figure 8.6 and Figure 8.7 is 0.005 seconds. My results shows that for time differences smaller than this value there are only minor changes in the various measures being looked at (except for the force total force on the slider). Hence, there is no need to examine results at smaller time intervals than this, because the images do not provide any greater insights.

At $t_3 = 2.055$ seconds we notice a major difference for most of the measures. The velocity field has become much more uniform for most of the slider. This is possibly due to the big increase in number of contacts with the base. Because earlier on there were fewer contacts, parts of the slider was able to sustain a higher velocity for a longer period. Now with more contacts causing more friction, parts of the slider is slowed down. The same kind of pattern can be observed for the shear forces, where we see that the overall force on each element in contact with the slider is approximately the same.

For the normal force we see that this is not the case. There is a much greater spread in values for the normal force on each element compared to the shear force. The dissipation is comparatively greater than shown in previous figures, and can be linked to the further increase in the number of contacts.

As the slider keeps moving along the track, the number of contacts begin to decease. In Figure 8.9 at $t_4 = 2.137$ we see that there is only a single contact left between the base and the slider.

We have to move approximately 0.04 seconds ahead in time before we begin to see a noteworthy increase in the number of contacts again. This gradually take us to a situation similar to the one in Figure 8.6 and repeat the entire cycle described in Figure 8.6 to Figure 8.9, but with a small degree of variations. My results indicate that such at cycle repeat roughly every 0.15 seconds.

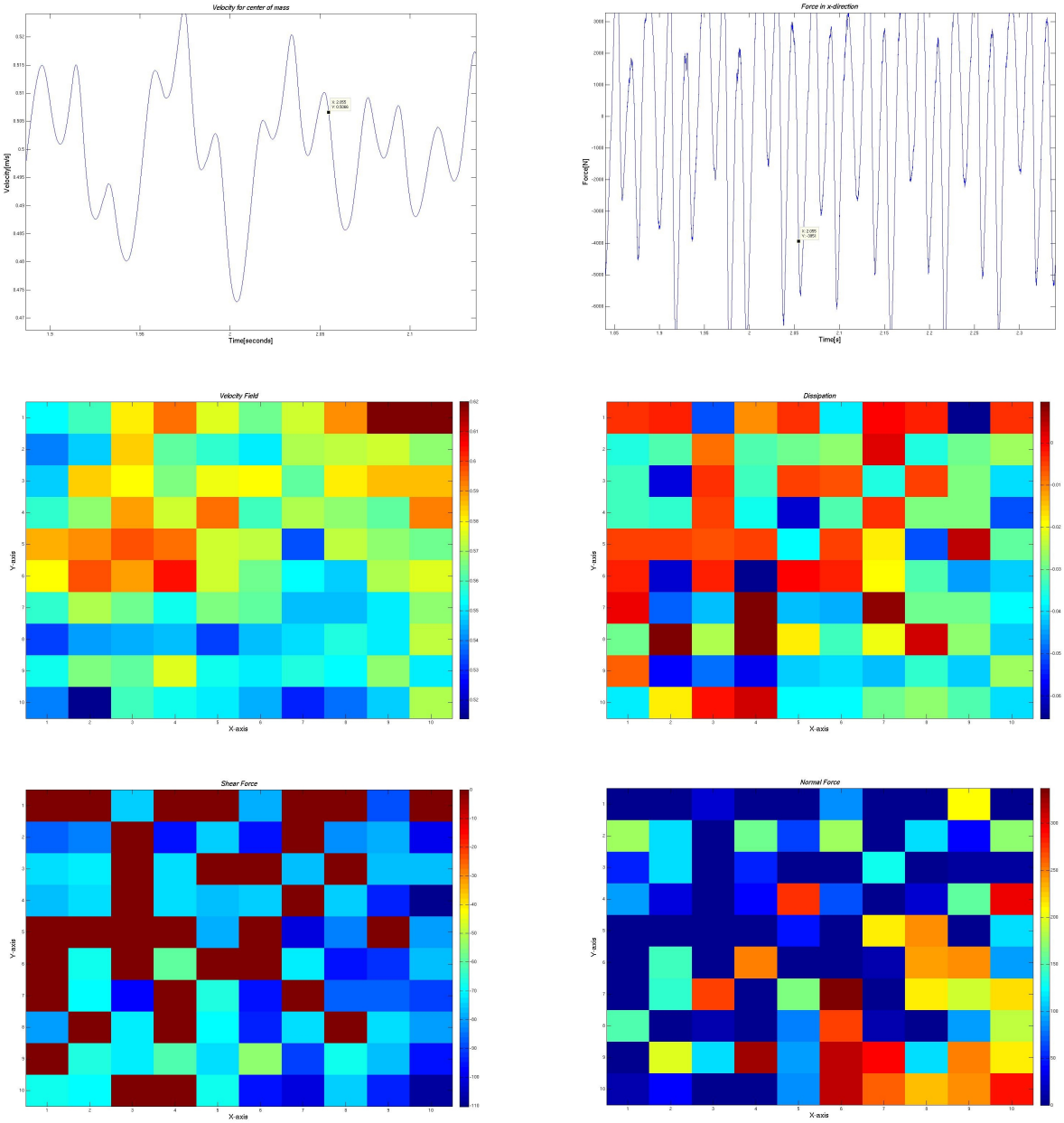

Figure 8.8: System at $t_3 = 2.055$ seconds

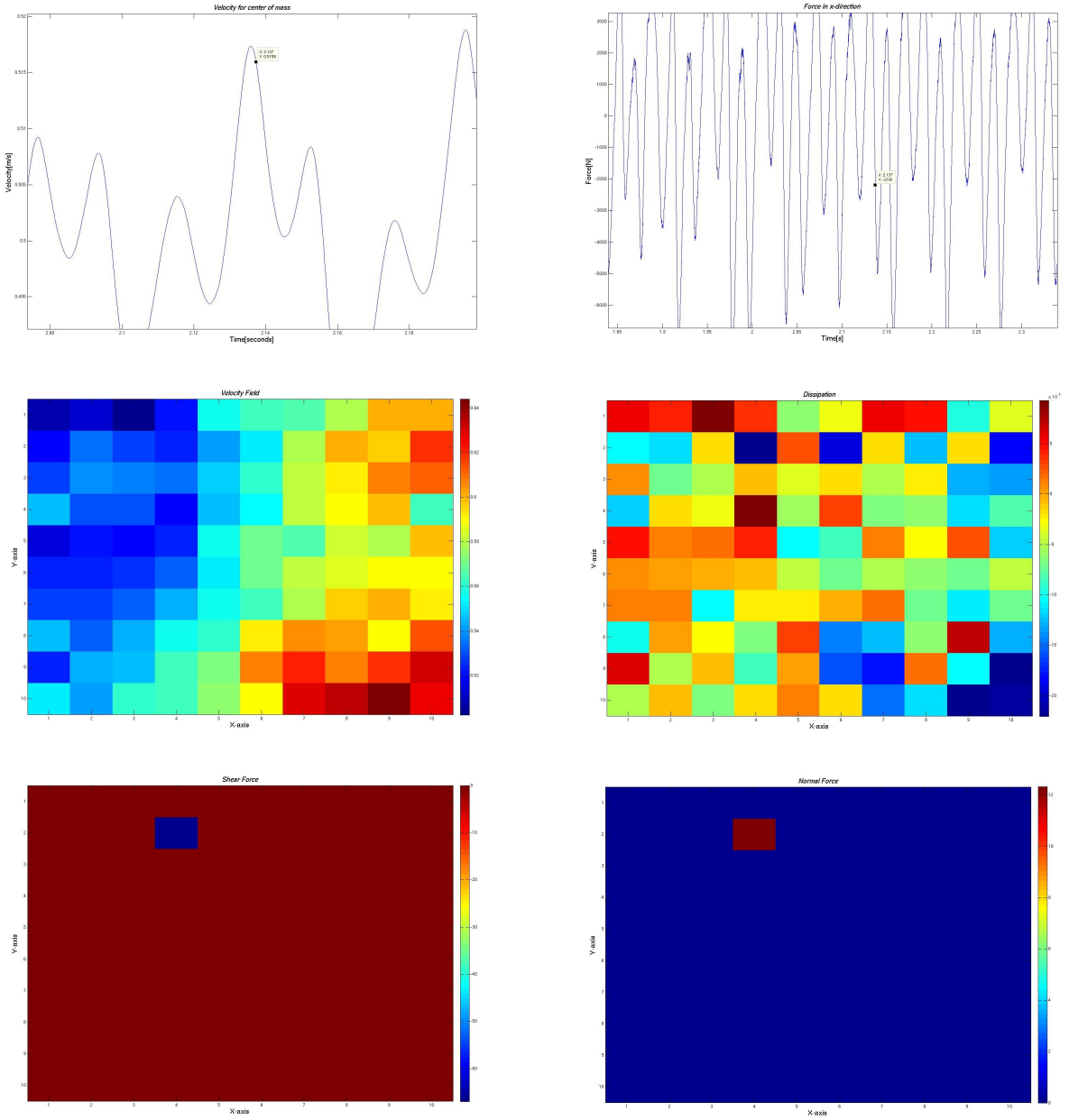

Figure 8.9: System at $t_4 = 2.137$ seconds

8.3 Summary of observations

There seems to a repeating behaviour for most of the measures I have used over the time-scale I looked at

- **Velocity for center of mass**
  As stated earlier, this value varies in a semi-periodic pattern over time. It shows that slider is not moving at a fixed velocity, but is constantly speeding up and down.

- **Force on the slider from the piston**
  This value has the most rapid variation in time, but along with the mass center's velocity has the most steady behaviour. Looking at this value helps me predict when the slider will speed up or down.

- **Velocity field**
  By looking at the velocity field I am able to tell how each part of the slider's base is moving. My observations indicate that at different times, various parts of the slider move at different velocities. These parts could be divided into sub-regions of varying sizes. I also noticed that neighbouring particles did not necessarily have the same relative shift in velocity over time. This clearly indicates that such particles do not necessarily displace the same distance for a given time. It should also be noted that at times the left and the right half of the slider had a marked difference in velocity.

- **Dissipation**
  For the most part the change in dissipation over a given time interval was consistent as long as the number of contacts were sufficient. Clearly there is a connection between where the base and the slider and are in contact with the areas where the most energy is dissipated.

- **Shear force**
  The shear force gives much of the same information as the change in dissipated energy, but provides an instant image of the contact population.

- **Normal force**
  The normal force also gives much of the same information as the dissipation and shear force. But as I noted earlier the variation in normal

force is generally less than for the shear force. I also saw indications of that in larger areas where the normal force was zero an increase in the velocity-field would manifest at a later time.

None of the measures I have used is single-handedly able to provide a satisfactory account of the events taking place during the sliding motion. By comparing the measures with each other at various points in time, I am able to extract a great deal of information and make useful observations that help me describe the sliding process.

8.4 A critical view

8.4.1 The model

Because friction is both a macroscopic and microscopic process, realistic simulations are nearly impossible. It is more than likely that the macroscopic effects of friction are microscopic in origin. As stated earlier the model I have used is a relatively simplistic one and there are several things that could be improved to make it more realistic:

- **Wear effects**
  In all natural phenomena involving friction inevitably results in some kind of wear and tear. Therefore it might have been useful to allow breakage of contacts within the slider to simulate such effects. But then again one might argue that considering the time-scale and system size these effects would be negligible

- **The Base**
  Although I have simulated roughness along the track is probably not sufficient for a realistic representation since this roughness only occurs at a single length-scale versus real systems that have roughness on several length-scales.

- **State and rate effects.**
  None of the aforementioned state and rate dependent effects are taken into account in my model(for example asperity creep).

- **Heat effects.**
  As mentioned I have disregarded heat effects because they supposedly

do not make much of a difference. But for larger systems and faster sliding velocities it would be useful to have this feature.

Ultimately, in my view the model only serves as a crude view of what is a highly complex phenomena. Nevertheless, it does captures the essence of friction and provides some useful results and insights.

8.4.2 Sources of error

There are many possible sources of error along the way. One obvious problem is that the colour-bars in some of my figures are rescaled for each time-frame that I looked at. This naturally created problems when interpreting the results. On the other hand, the amount of rescaling done was minimal and by a thorough investigation the influence of this problem was kept to a minimum. Also, because I used the tracing tool found in Matlab to mark the points being looked at there is a small degree of inaccuracy being introduced to my results, but not enough to give misleading results.

Chapter 9

Results for onset of sliding

In light of the findings by Rubinstein et al. and Zapperi et al. discussed in Section 2.5 it would be interesting to compare my results with theirs. Specifically, I would like to see if I can observe some the same detachment fronts described at the onset of sliding, as well as soundwawes during initial sliding. The other thing I want to examine is if a local slip event in my model also grows into a global slip as observed by Zapperi et al.

9.1 Recalibration

In the previous chapter I examined the dynamics that take place on a timescale given by the sliding velocity. However, there is another timescale defined by the velocity at which a soundwave propagates in the material of the slider. If I want to observe wave phenomena moving at such speeds, I will have to readjust my time-step. Theoretically this should give me a high enough resolution, so that I can capture these disturbances and slip events. From [3] we know that the sound speed in a lattice with spring connections k_1 and k_1 where $k_1 > k_2$ is given by

$$v_s = \sqrt{\frac{k_1}{m_0}} l_0 \tag{9.1}$$

where l_0 is the lattice constant and v_s is the speed of sound in the solid.

Alternatively I can use the definition:

$$v_s = \sqrt{\frac{E}{\rho}} \tag{9.2}$$

where E is Young's modulus and ρ is the mass density of the material.

The value of the timestep must be small enough to resolve the appropriate dynamics. Therefore, it should be considerably less than the time it takes for a soundwave to travel from one lattice element to the next. That is $\Delta t << \frac{l_0}{v_s}$. From calculations I find that a soundwave should move at $v_s = 1000m/s$ in the slider. Comparatively, the driving velocity is $0.5m/s$. I may also have to readjust some of the other parameters like the gravity, considering the relatively low mass of the slider. Excessive values for gravity will end up effectively chocking movement. Conversely, a too small value will not generate enough friction.

9.2 Motion of the slider

As one can see from Figure 9.1, the slider is initially motionless at the start of the simulation. There are mainly two regions of interest, that are demarcated by the two boxes in Figure 9.2. In the first region one can observe a rapid build-up for the force experienced by the slider, setting it into motion. During this phase the slider experiences the greatest acceleration and is speeding up. In the second region the slider is subject to a smaller series of impacts and is gradually slowing down, but the sliding velocity has not become stable yet. In Figure 9.3 and the variations in the slider's energy decreases gradually.

Initially I look at two measures to determine how the slider moves in the two regions. Namely, the velocity field and a displacement profile. The displacement profile is created from the movement for an interval of 10 timesteps for the bottom layer of the slider. So the specified timestep in the displacement profiles indicate how many meters (on the x-axis) each of the 10 particles have been displaced from their respective rows (numbered back to front on the y-axis) during the interval.

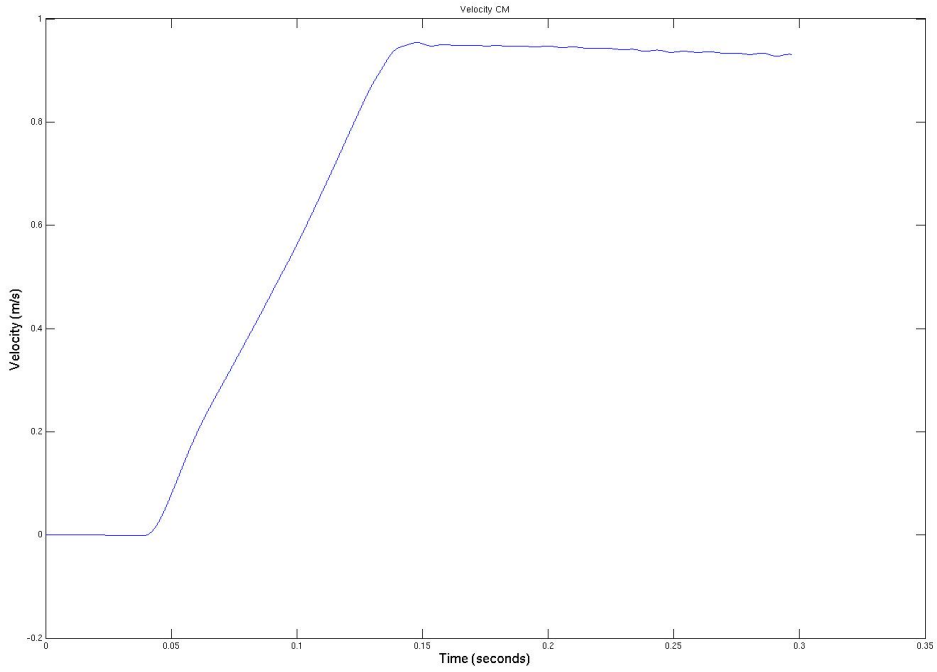

Figure 9.1: Velocity for center of mass

9.2.1 Region 1

The changes in the velocity field preceding the time at which this region starts are minimal, and the displacement profile during this period indicate little or no movement. Inside the first region where the onset of sliding takes place, one can see a wavefront spreading out in the x-direction. This is noticable in both of the applied measures, Figure 9.5 and Figure 9.6. It takes approximately 30000 timesteps for this wave to move from the back of the slider to the front. For the velocity field plots on can observe that all the particles on the same row (in the y-direction) have approximately the same velocity. The displacement profiles reveal that there is also a small difference in the amount across each row. This is probably due to very small oscillations in the slider.

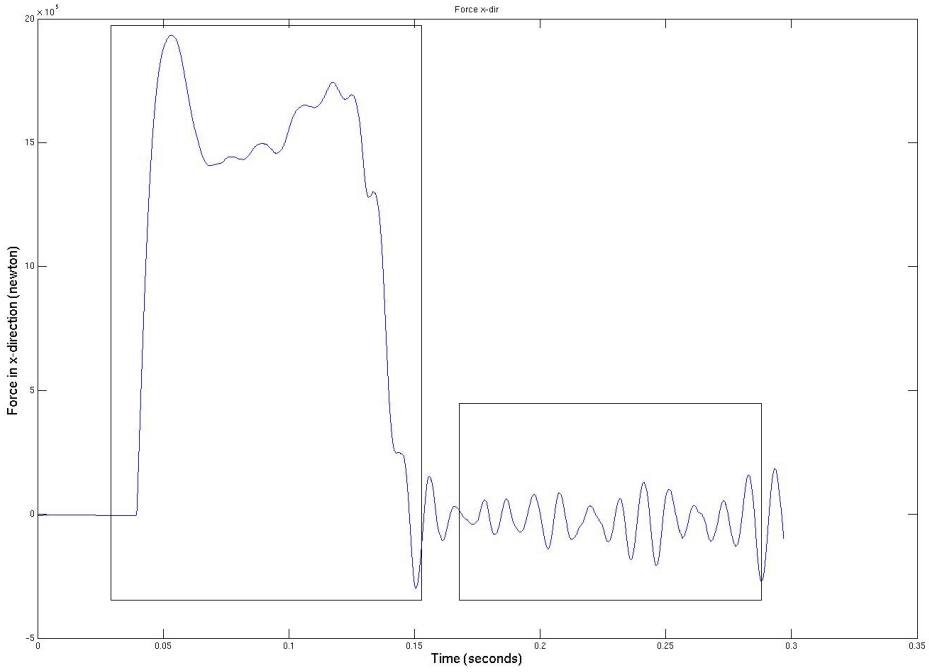

Figure 9.2: Force on slider

9.2.2 Region 2

In this region, the entire slider is in motion as seen in Figure 9.7 and Figure 9.8. Here one can also observe semi-periodic waves being emitted and reflected in different directions. A high degree of symmetry was also observed for many of these waves. One can see from the displacement profiles that the overall displacement is greater than in the previous region. But still the overall behaviour along the rows are similar, and there is an oscillating pattern going back and forth.

9.2.3 Variations in normal force

Here I take a look at the changes in normal force for both the regions, for individual slider particles and their sum as a function of time. Figure 9.9

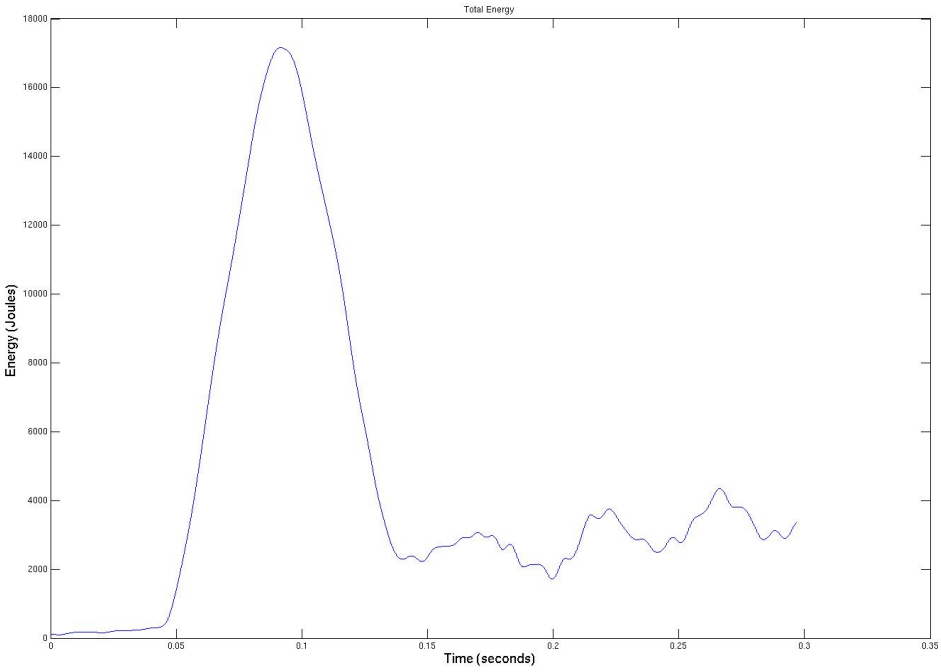

Figure 9.3: Energy of slider

and Figure 9.10 shows that there are very large fluctuations in the normal force for both regions. In region 1 the slider starts to lose contact with the base as the wavefront moves through the slider, so one can see a connection when comparing plots of the velocity field and normal force in this region.

For region 2 it is much more difficult to see an immediate connection between the plots of the velocity field and normal force. Figure 9.11 shows that throughout the motion of the slider there is a continuous oscillation in the normal force. I suspect that this is due to a torque around the y-axis, possibly stemming from the combination of overlapping slider and substrate particles. The oscillations continue to dominate to motion of the slider. The torque creates a sort of jumping motion jumping motion along the track, where the front and the back of the slider alternates between hitting the substrate.

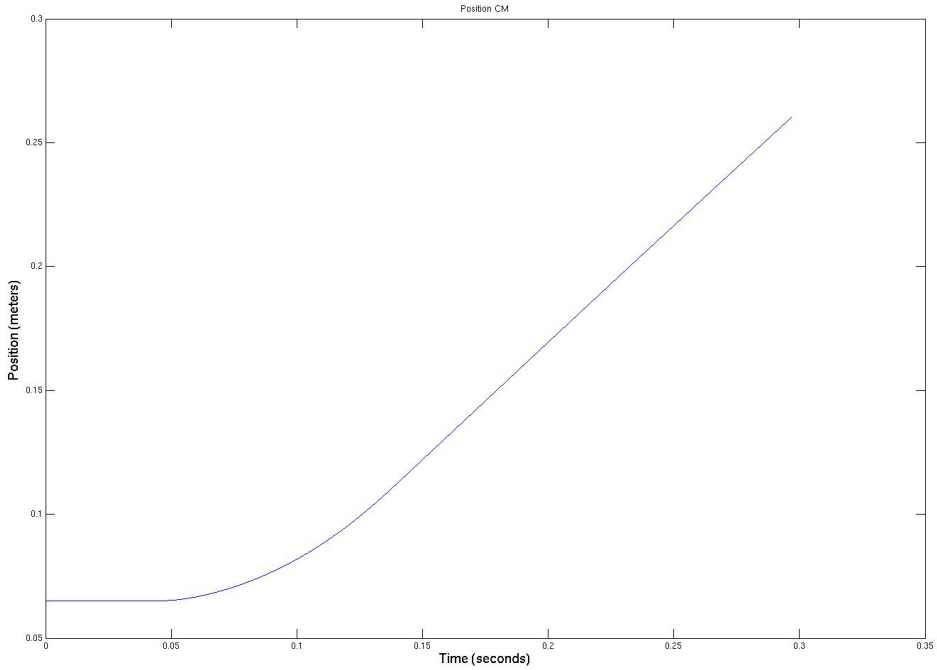

Figure 9.4: Position of center of mass

9.2.4 Calculations and remarks

There are some useful quantities that can be extracted from the various plots. Particularly, I am interested to see at what speed the initial front observed in region 1 moves at. Originally I suspected that the front might be either a soundwave or just the driving velocity. However calculations for this region show that the speed of the front is $2.5m/s$, which is neither of the above. I also estimated the speed of front in region 2. Here I found that a typical front in this region moves at around $4.3m/s$ Finally, I estimated the frequency for oscillations in the normal force for both the regions, seen in Figure 9.12 and Figure 9.13. My calculations show that the one of the oscillations in region 1 has a frequency of around $64.59Hz$ and $91.19Hz$ for region 2. I have no immediate answer to why the speed of the fronts are what they are, and I

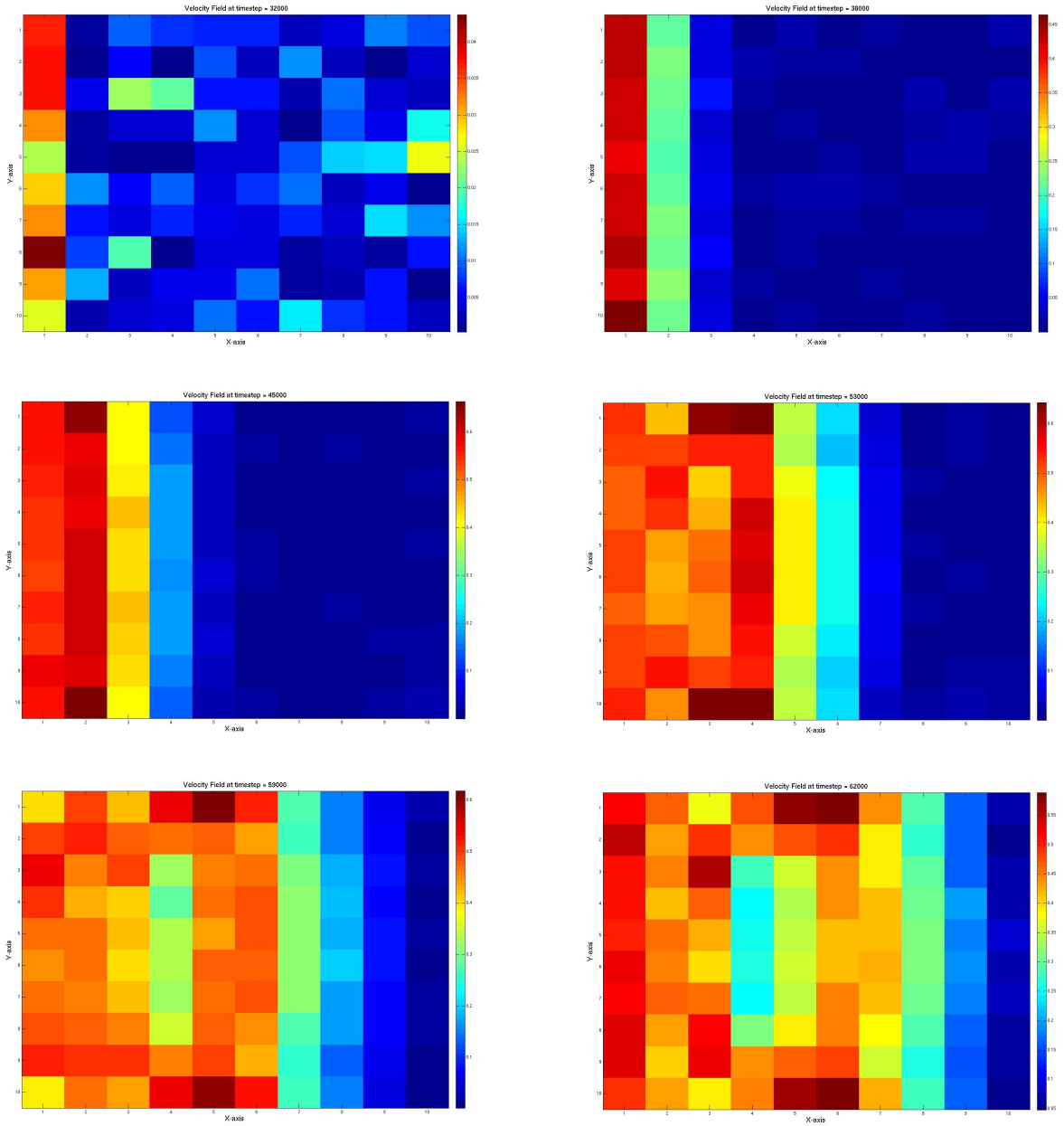

Figure 9.5: Velocity field from region 1

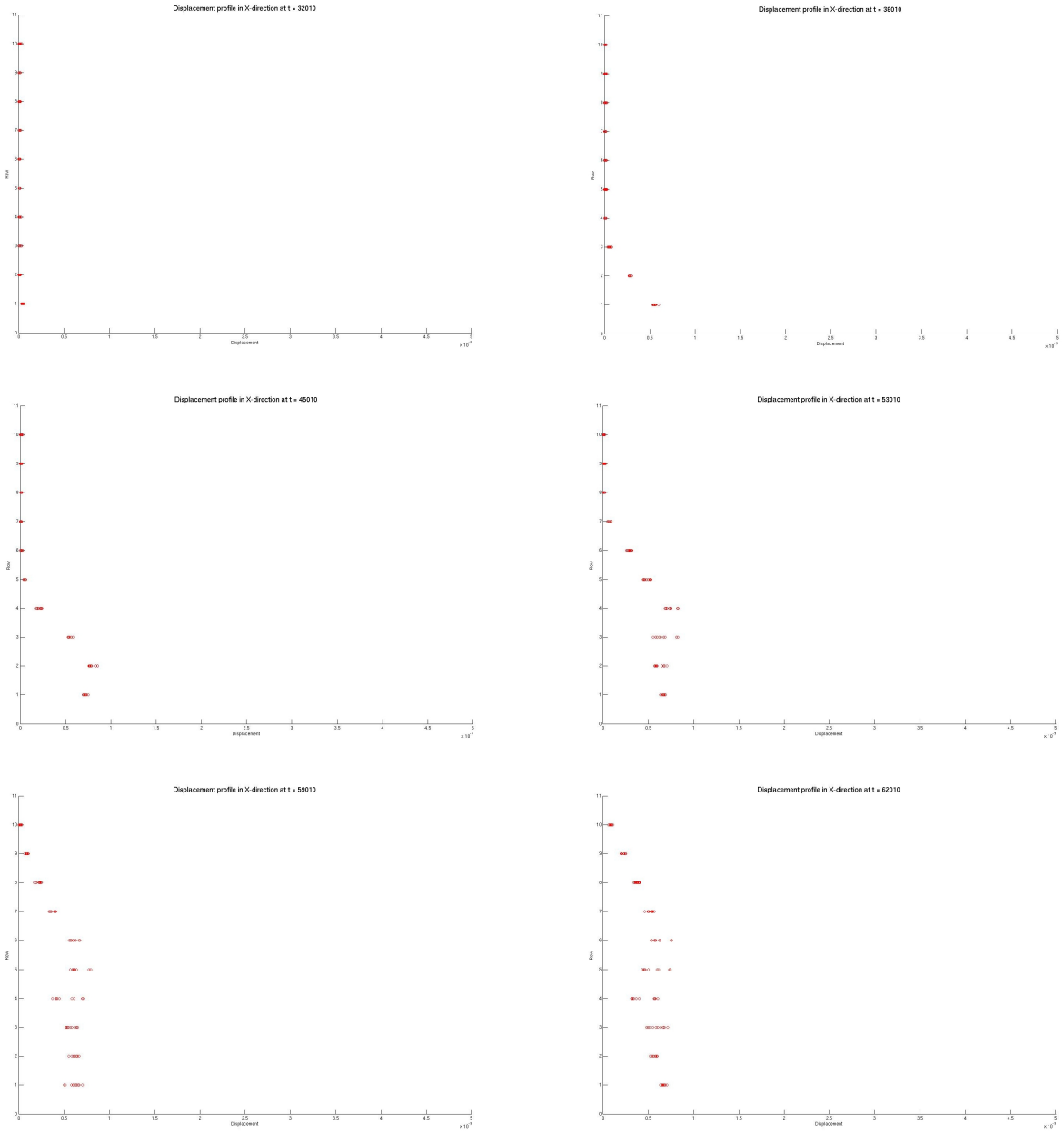

Figure 9.6: Displacement profile from region 1

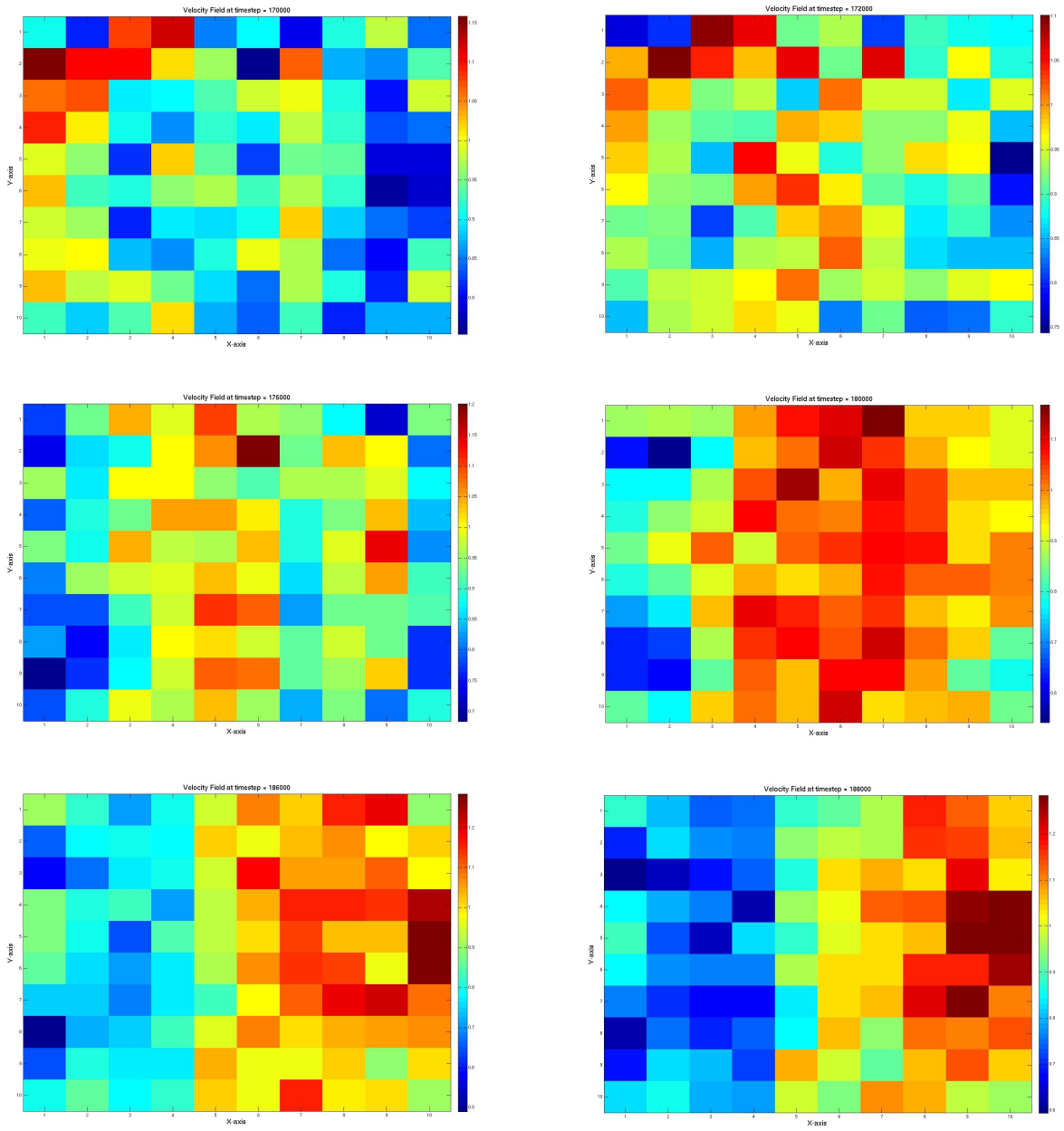

Figure 9.7: Velocity field from region 2

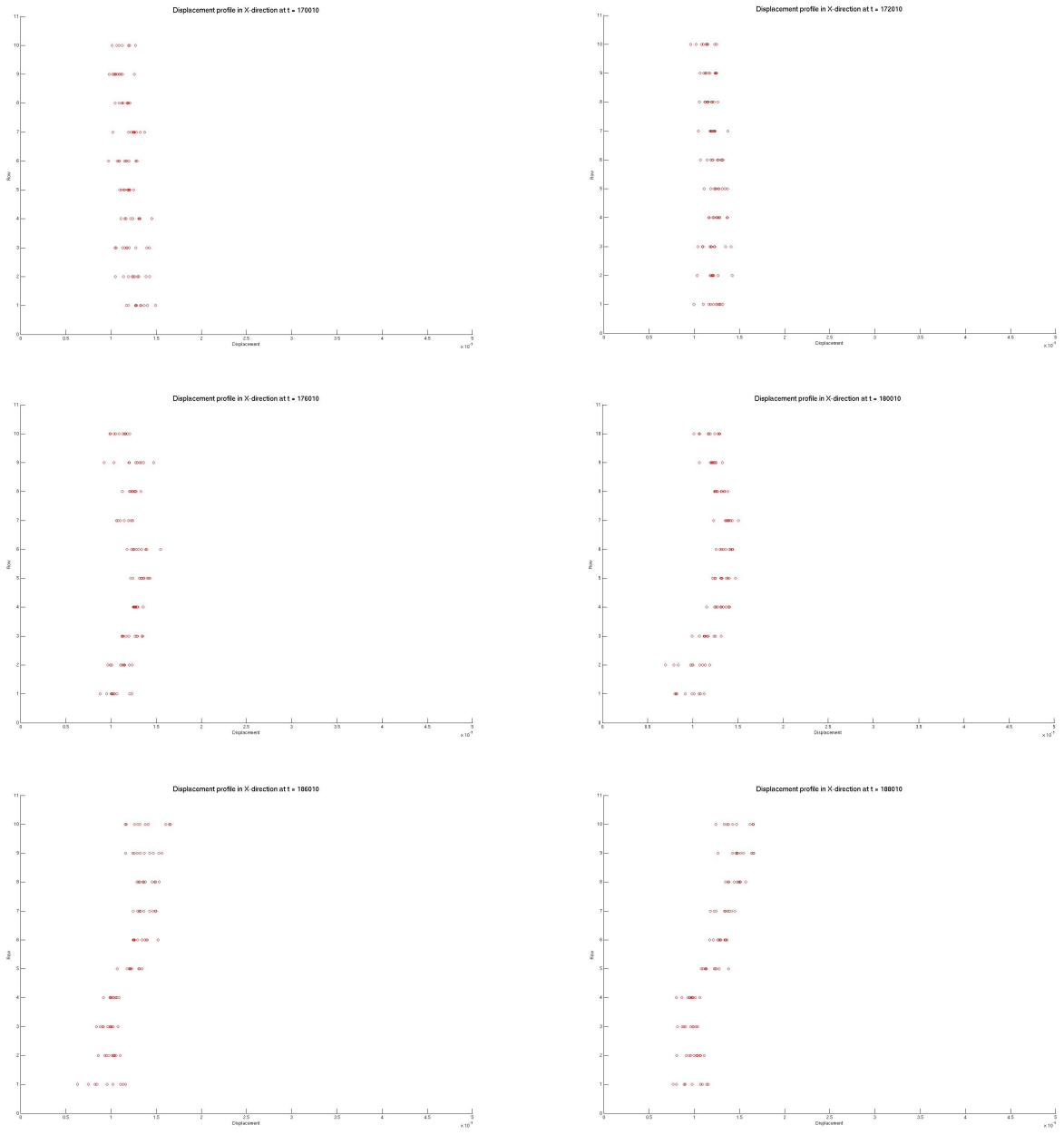

Figure 9.8: Displacement profile from region 2

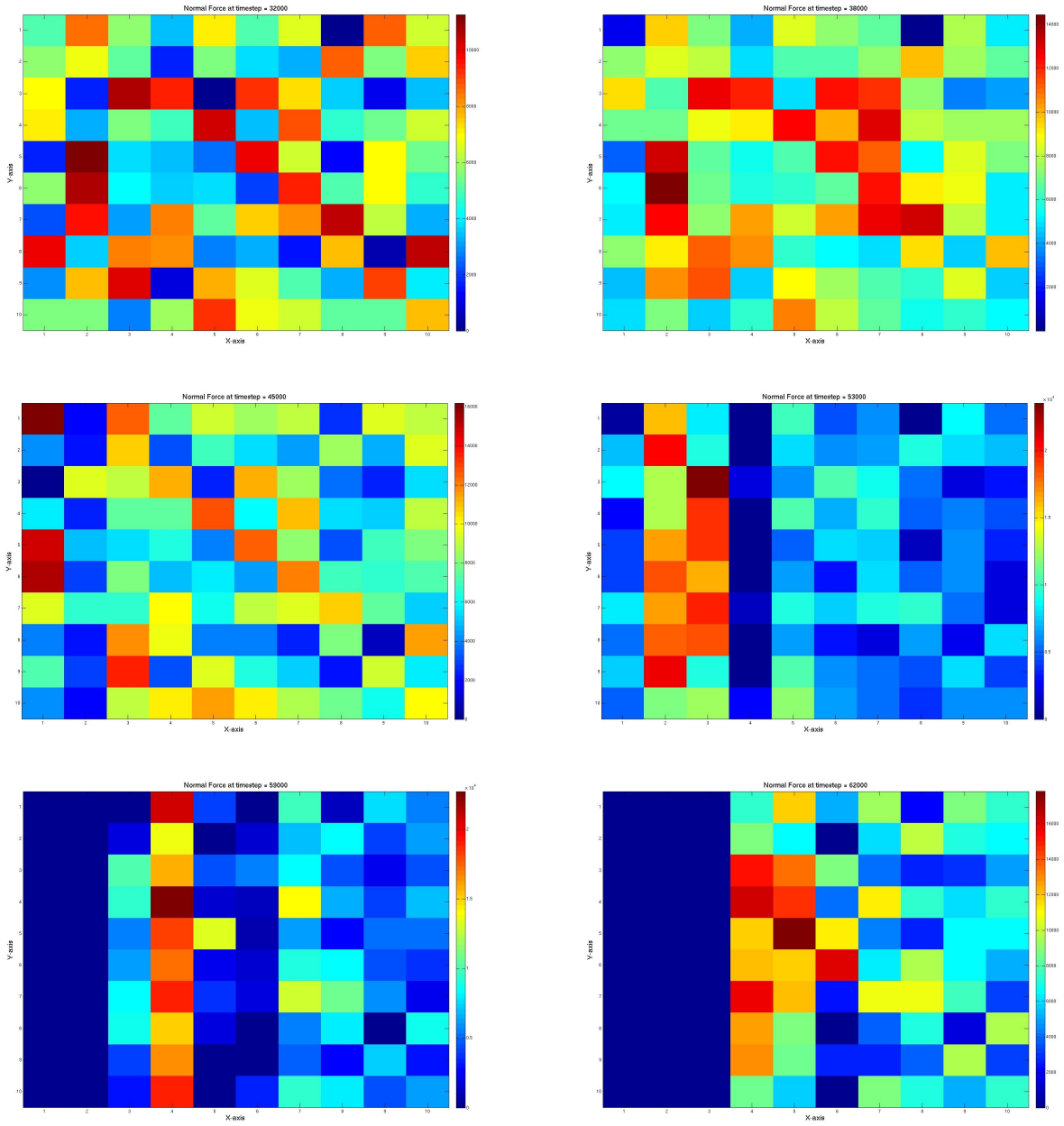

Figure 9.9: Normal force from region 1

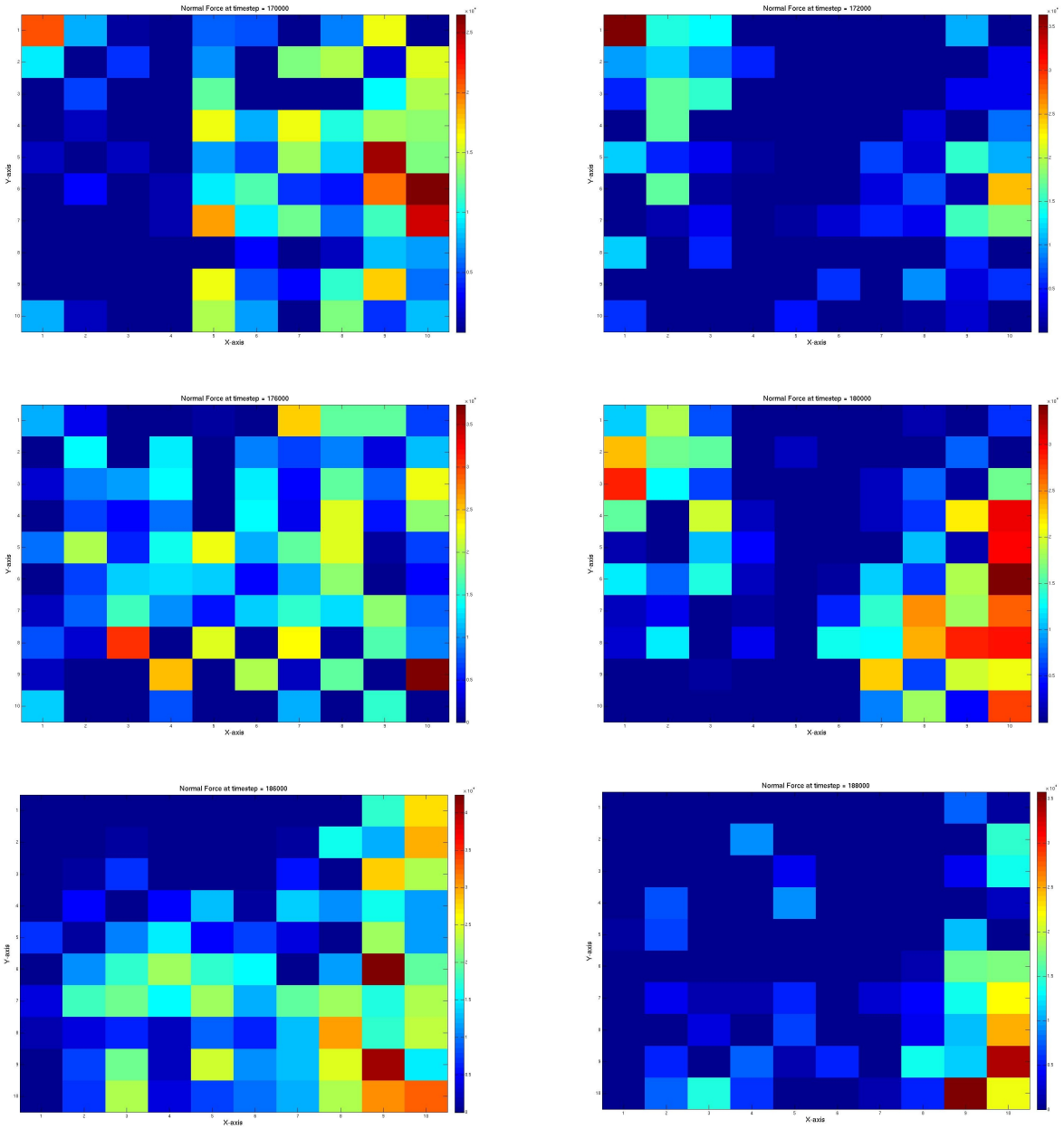

Figure 9.10: Normal force from region 2

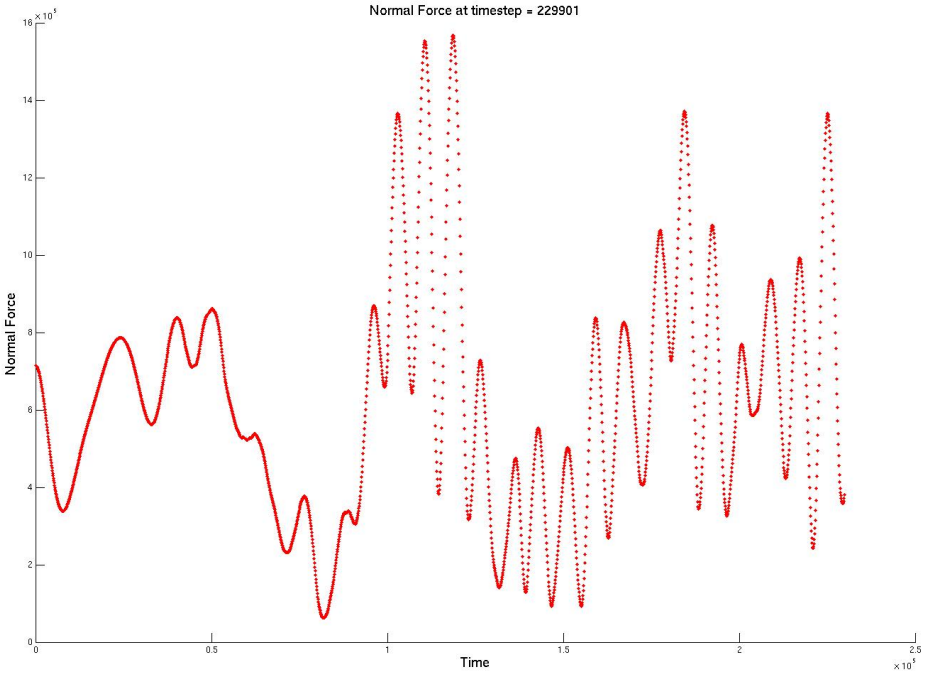

Figure 9.11: Oscillations in normal force

can only speculate until I have conducted further investigations. Although I was unable to observe any soundwaves I did see possible indications of that a small slip event can grow into larger ones. These are easiest to spot when scrolling through plots of the velocity field.

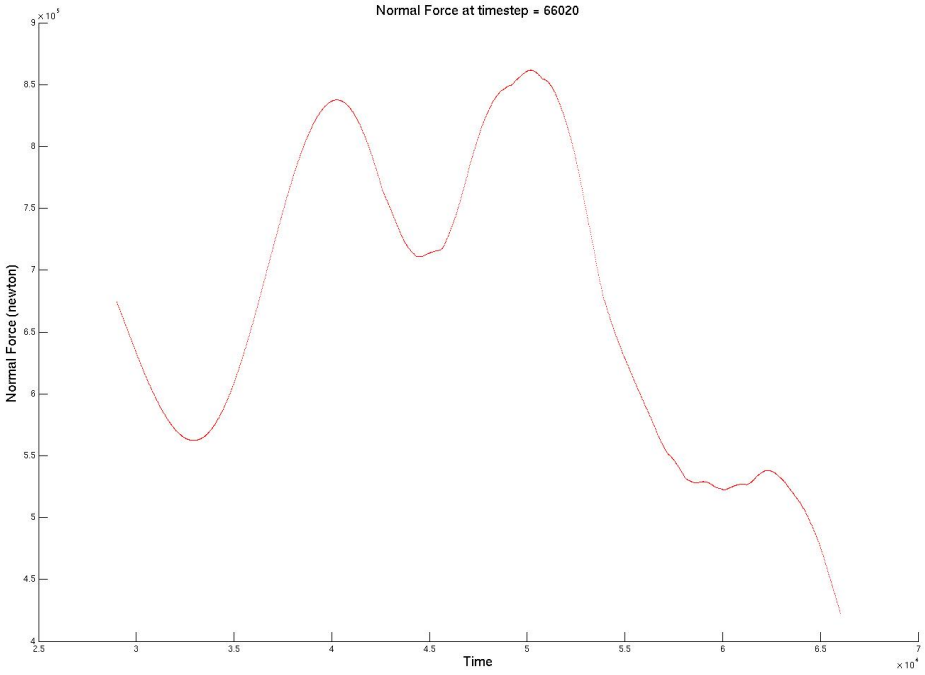

Figure 9.12: Oscillations in normal force from region 1

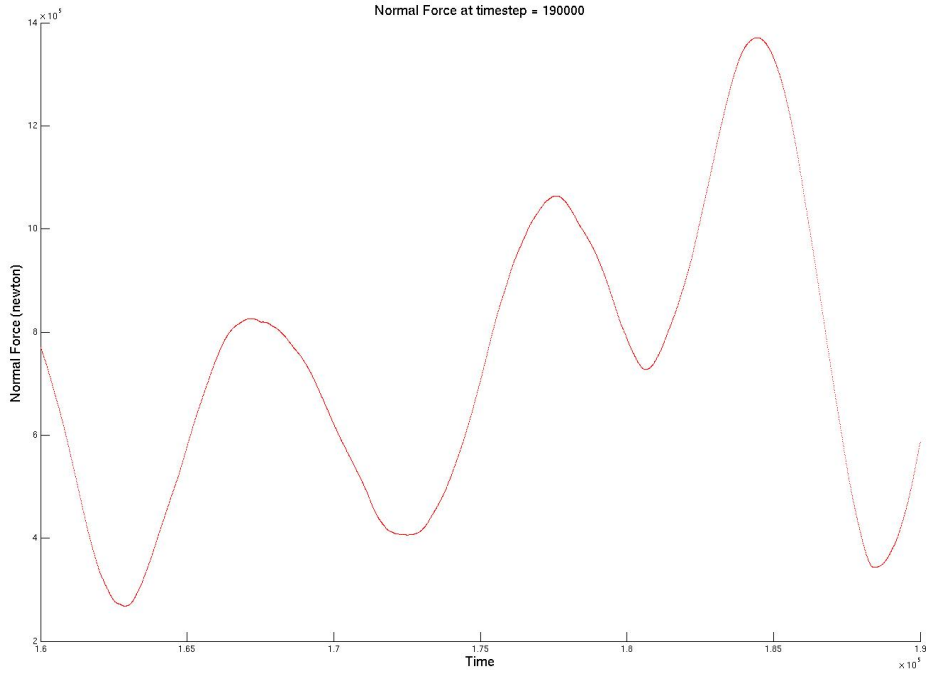

Figure 9.13: Oscillations in normal force from region 2

Chapter 10

Final thoughts

The majority of the allotted time for this project was used to make sure that the system was robust and writing and testing code for a flexible system. The code is written in C++ and uses Paraview for visualization and its various toolboxes. Debugging was done by looking directly at the numerical output and animations of the system. Selecting a decent set of values for the parameters also proved difficult, specially for a system that should respond according to expected behaviour.

Much of the work I did went into testing the program. A major reason for this was that I had to replace several algorithms in the program in an attempt to track down errors. Of course this entailed more testing. Ultimately this left me less time to produce and analyze my final results. Ideally I would also have liked to compare my results with larger systems for a range of other parameters and investigated adhesion effects.

In the end, this model has proven to be an adequate for my experiments. Through the development and application of my program I have been able to gain insight and uncover how the base of a slider moves. We have seen that a block apparently moving along smoothly, does not. Infact the base can be divided into sub-regions that slip a separate intervals.

Bibliography

[1] Baumberger, Caroli Solid friction from stickslip down to pinning and aging. Advances in Physics Vol. 55 Jun 2006,

[2] Chris Marone LABORATORY-DERIVED FRICTION LAWS AND THEIR APPLICATION TO SEISMIC FAULTING. Annu. Rev. Earth Planet. Sci. 1998.26:643-696,

[3] Ruth W. Chabay,Bruce A. Sherwood Matter and Interactions 2002.

[4] Reguzzoni, Marco and Ferrario, Mauro and Zapperi, Stefano and Righi, Maria Clelia Onset of frictional slip by domain nucleation in adsorbed monolayers..

[5] Andy Ruina Slip Instability and State Variable Friction Laws

[6] D. Atack and D. Tabor. The friction of wood. *Proceedings of the Royal Society of London. Series A, Mathematical and Physical Sciences*, 246(1247):pp. 539–555, 1958.

[7] J H Dieterich and B Kilgore. Implications of fault constitutive properties for earthquake prediction. *Proceedings of the National Academy of Sciences of the United States of America*, 93(9):3787–3794, 1996.

[8] James H. Dieterich and Brian D. Kilgore. Direct observation of frictional contacts: New insights for state-dependent properties. *Pure and Applied Geophysics*, 143:283–302, 1994. 10.1007/BF00874332.

[9] Jianping Gao, W. D. Luedtke, D. Gourdon, M. Ruths, J. N. Israelachvili, and Uzi Landman. Frictional forces and amontons' law: From the molecular to the macroscopic scale. *The Journal of Physical Chemistry B*, 108(11):3410–3425, 2004.

[10] Sangil Hyun and Mark O. Robbins. Elastic contact between rough surfaces: Effect of roughness at large and small wavelengths. *Tribology International*, 40(10-12):1413 – 1422, 2007. Tribology at the Interface: Proceedings of the 33rd Leeds-Lyon Symposium on Tribology (Leeds, 2006).

[11] K.C Ludema. *Friction, Wear, Lubrication*. CRC Press, 1996.

[12] Yu. M. Mamontova and A. S. Akhmatov. Departures from amonton's law of friction. *RusVol. 55sian Physics Journal*, 17:1553–1556, 1974. 10.1007/BF00891111.

[13] Hiroshi Matsukawa and Hidetoshi Fukuyama. Theoretical study of friction: A case of one-dimensional clean surfaces. 1994.

[14] Meyer. *Nanoscience; Friction and Rheology on the Nanometer Scal*, volume 1. 1998.

[15] Delphine Gourdon Michael Urbakh, Joseph Klafter and Jacob Israelachvili. The nonlinear nature of friction. *Nature*, 430, 2004.

[16] Akihiro Nishimoto, Tsuyoshi Mizuguchi, and So Kitsunezaki. Numerical study of drying process and columnar fracture process in granule-water mixtures. *PHYSICAL REVIEW E 76, 016102*, 2007.

[17] G. Ouillon and D. Sornette. Long-range static directional stress transfer in a cracked, nonlinear elastic crust. *Future Generation Computer Systems*, 22(4):500 – 520, 2006.

[18] S. M. Rubinstein, G. Cohen, and J. Fineberg. Contact area measurements reveal loading-history dependence of static friction. *Phys. Rev. Lett.*, 96(25):256103, Jun 2006.

[19] S M Rubinstein, G Cohen, J Fineberg, and M Shay. Crack-like processes governing the onset of frictional slip. (cond-mat/0603528), Mar 2006.

[20] Gil Cohen and Jay Fineberg Shmuel M. Rubinstein. Detachment fronts and the onset of dynamic friction. *Nature*, 430, 26 August, 2004.

[21] Zhiping Yang, H. P. Zhang, and M. Marder. Dynamics of static friction between steel and silicon.

[22] Hugh D. Young, Roger A. Freedman, and Francis W. Sears. *University physics : with modern physics.* Addison Wesley, 2008.